BACHELOR THESIS

MICROMETER SCALE 3D MEMBRANE PRINTING TOWARDS LOCUST EAR IMITATION

Jort Verhaar

ELECTROTECHNIEK, WISKUNDE EN INFORMATICA
TRANSDUCERS SCIENCE AND TECHNOLOGY

EXAMINATION COMMITTEE
Prof. Dr. Ir. Gijs Krijnen
Dr. Ir. Tom Vaneker
Dr. Herman Hemmes (Interim Chairman)

UNIVERSITY OF TWENTE.

MAY 2015

Symbols

Symbol	Definition	Unit
a	Center point of the membrane	m
a	Location of beam connection	m
A	Area	cm
b	Length of rotational beam	m
C	Arbitrary constant	-
C_{b}	Bulk concentration	$\mathrm{mg\,cm^{-3}}$
C_{s}	Saturation concentration	$\mathrm{mg\,cm^{-3}}$
d	Boundary layer thickness	cm
d	Thickness	m
D	Bending stiffness	$\mathrm{kg\,m^2\,s^{-2}}$
D	Diffusion coefficient	$\mathrm{cm^2\,s^{-1}}$
D	Location down	-
D	Thickness	m
D_0	Diffusion coefficient at infinite temperature	$\mathrm{cm^2\,s^{-1}}$
e	Displacement of scale	m
E	Young's modulus	Pa
E_{A}	Activation energy for diffusion	$\mathrm{J\,mol^{-1}}$
F	Force	N
h	Height	m
J	Diffusion flux	$\mathrm{mg\,cm^{-1}\,s^{-1}}$
k	Dissolution rate constant	$\mathrm{cm\,s^{-1}}$
k	Integration constant	-
k	Boltzmann constant 1.3806×10^{-23}	$\mathrm{J\,K^{-1}}$
k	Spring constant	$\mathrm{N\,m^{-1}}$
l	Length	m
m	Mass	mg
mw	Molecular weight	kg
N	Tension force per unit length	$\mathrm{N\,m^{-1}}$
p	Uniformly distributed pressure	$\mathrm{N\,m^{-2}}$
P	Point load	N
P	Pressure	$\mathrm{N\,m^{-2}}$

P_v	Vaporization pressure	$\mathrm{N\,m^{-2}}$
r	Radial point on the membrane	m
r	Radius	m
R	Gasconstant 8.3144	$\mathrm{J\,mol^{-1}\,K^{-1}}$
R	Ratio between membrane and plate behavior	-
t	Time	s
T	Location Top	-
T	Tension	N
T	Temperature	K
u	Displacement	m
V_m	Volume of material	$\mathrm{cm^3}$
V_s	Volume of solvent	$\mathrm{cm^3}$
w	Deflection of the membrane	m
w_0	Maximum deflection at the center of the membrane	m
w	Width	m
α	Angle between the deflected and non-deflected membrane at the rim	-
ϵ	Strain	-
ϵ	Integration variable	-
θ	Angle on the membrane	rad
λ	Wavelength	$\mathrm{m^{-1}}$
ν	Poisson ratio	-
ρ	Density	$\mathrm{kg\,m^{-3}}$
ω	Angular frequency	$\mathrm{s^{-1}}$
ω_0	Resonance frequency	$\mathrm{s^{-1}}$
σ	Stress	$\mathrm{N\,m^{-2}}$
σ_T	Intrinsic stress	$\mathrm{N\,m^{-2}}$
ϕ	Concentration per unit volume	$\mathrm{mg\,cm^{-3}}$
∇	Differential Operator del	-

Contents

Chapter 1

Introduction

In this report possibilities to mimic a Locust Ear membrane with 3D print technology will be investigated. 3D print technology is widely used for single piece production, rapid prototyping and research purposes. These different applications and specific usages lead to different printing techniques with their own advantages and disadvantages. In this report the process from design towards fabrication and measurements is described.

The fabrication of micrometer scale structures is hardly scientifically done or reported. Therefore crucial design parameters are not documented in literature and have to be found. During the manufacturing process problems arise, which are dealt with in this report. Creation of membranes is earlier done by Pieter Westrik [2] in silica. Now his work is elaborated for the creation of 3D printed membranes.

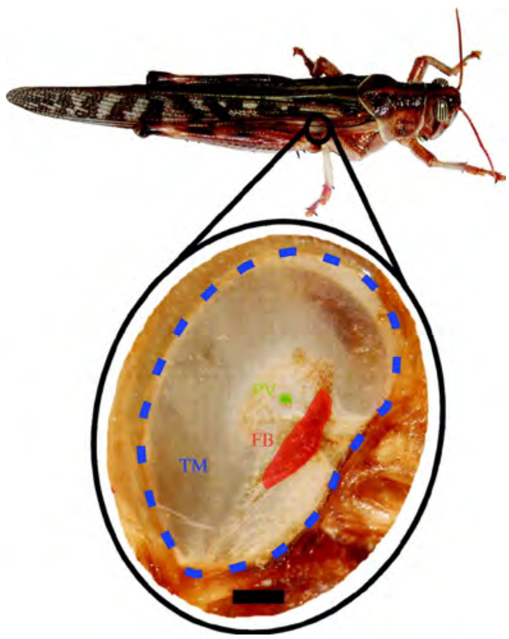

FIGURE 1.1: Tympanal organ of a Locust [1]

1.1 Locust Ear

The locust ear consist of a complex organ with a membrane which is able to discriminate different frequencies in the sound field. This membrane is called the tympanal membrane. It consists of a thin part and a thicker part. Four groups of receptor cells are attached to four specialized areas in the membrane. The incoming traveling waves propagate over the membrane towards the receptor cells. These cells have a maximum sensitivity for the resonance frequency at that location. In figure 1.1 the tympanal organ is pictured. In blue the tympanal membrane is marked, in red the region with neurons sensing below 10 kHz and in green the region with neurons sensing above 10 kHz. Thicknesses around the membrane guide the waves and separate the different frequencies. The different resonance peaks are analyzed and used to regenerate the sound-spectrum of interest. In this way nature gives us inspiration for new energy efficient sensors. [3, 4]

1.2 3D Printing

Rapid prototyping, additive manufacturing or 3D printing is a construction method to generate models on small scale. One of the advantages of the method is that it is possible to produce single items, therefore pieces can be designed specifically for their purpose. This is useful in this setting, to be able to design membranes for a specific frequency range. This production process is much faster than creating structures using microelectromechanical systems (MEMS), which makes it suitable for research purposes and fast applications. MEMS are widely used in sensor technology and earlier in membrane design.

Fused deposition modeling prints multiple layers of material on top of each other. The technology behind 3D printing evolves and makes it possible to print in thinner and thinner layer-thicknesses as well as constructing thinner walls. The basic principle of 3D printing is shown in figure 1.2 where the material is heated and extruded in lanes. The material cools down, and the platform lowers to make space for the new layer. The new layer is printed on top of the previous layers. More on techniques of 3D printing is written in chapter 4. The multilayered process gives abilities to create sensors in 3D instead of the currently used silica sensors. For the membrane sensors this means that it is possible to locally thicken the membrane, by adding lanes, triangles or circles, which guide the different waves over the membrane. Typical layer thicknesses are currently 100 μm and can be lower for specific printers. [6]

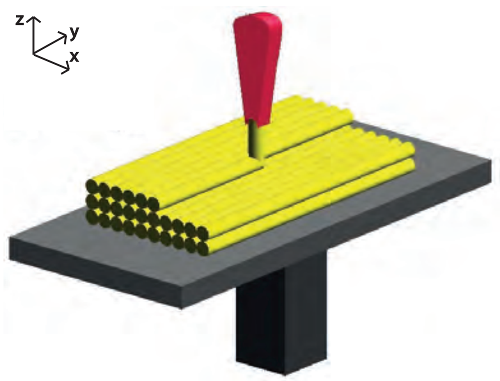

FIGURE 1.2: Fused Deposition Modeling [5]

In the production process the layers are build in a specific way. The layers are build up lane by lane in the y-direction and layer by layer in the z-direction. The material properties therefore can vary depending on the plane in which they are produced. This is important during the design of the membranes.

Chapter 2

Membrane Behavior

In this chapter the general theory behind vibrating membranes is explained. Different expressions for the characteristics of the membrane are derived to create an understanding of the behavior of the membrane. These derived expressions display the material properties needed and define the design parameters.

The characteristics of a membrane can be dominated by plate or membrane behavior. The difference between these two comes from the intrinsic tension applied to the membrane. When the intrinsic tension on the membrane is large the deflection is stress dominated and membrane behavior is observed. Plate behavior is dominated by the bending stiffness of the material. This results in different approaches when calculating the natural modes of the membrane.

The ratio between those two behaviors is given by 2.1. When R is much larger than 1, intrinsic tension dominates and membrane behavior would be expected. In the case R is much smaller than 1, bending stiffness dominates and plate behavior would be expected. [2] In the region around 1 a transition between both behaviors is observed.

$$R = \frac{3N^2(1-\nu^2)}{Ed^4\omega^2\rho} \tag{2.1}$$

Different shapes of membranes can be produced. All these shapes have their own advantages. The tympanal membrane has a kidney shape. This shape is harder to predict than symmetrical geometries. Therefore first simple geometries are considered. A cylindrical plate spreads stresses more evenly over the rim at the support. For a squared plate stresses deviate over the rim and the local stress can exceed the tensile strength. Resulting in ruptured membranes. Therefore cylindrical shaped plates are produced.

The natural frequencies give information on the characteristics of the membrane. It can be seen for which frequency range the membrane is sensitive and the type of behavior can be determined. Both these properties depend on the natural frequencies of the membrane.

2.1 Natural frequencies of a vibrating plate

The natural frequency for the membrane with plate behavior is calculated according to Soedel [7]. The plate is assumed to be homogeneous in material properties and circular in shape. To calculate the natural frequency of the plate, we start with the equation of motion in equation 2.2.

$$\frac{Ed^3}{12(1-\nu^2)}\nabla^4 w(r,\theta,t) + \rho d \frac{\delta^2 w(r,\theta,t)}{\delta t^2} = 0 \tag{2.2}$$

In order to solve the equation, 2.3 and 2.4 are applied to 2.2 to obtain 2.6. This substitution only holds for the natural frequencies, due to substitution 2.3.

$$w(r,\theta,t) = w(r,\theta)e^{i\omega t} \tag{2.3}$$

$$\lambda^4 = \frac{12\rho\omega^2(1-\nu^2)}{Ed^2} \tag{2.4}$$

$$\nabla^4 w(r,\theta) - \frac{12\rho\omega^2(1-\nu^2)}{Ed^2} w(r,\theta) = 0 \tag{2.5}$$

$$(\nabla^2 \pm \lambda^2)w(r,\theta) = 0 \tag{2.6}$$

The equation can be solved by separation of variables, giving equation 2.8 and 2.9.

$$r^2\left[\left(\frac{d^2R}{dr^2} + \frac{1}{r}\frac{dR}{dr}\right)\frac{1}{R} \pm \lambda^2\right] = -\frac{1}{\Theta}\frac{d^2\Theta}{d\theta^2} = k^2 \tag{2.7}$$

$$\frac{d^2\Theta}{d\theta^2} + k^2\Theta = 0 \tag{2.8}$$

$$\frac{d^2R}{dr^2} + \frac{1}{r}\frac{dR}{dr} + \left(\pm\lambda^2 - \frac{k^2}{r^2}\right)R = 0 \tag{2.9}$$

Solving equation 2.8 gives:

$$\Theta = A\cos(k\theta) + B\sin(k\theta) \tag{2.10}$$

If we now introduce a new variable to solve equation 2.9:

$$\varepsilon = \begin{cases} \lambda r & \text{if } \lambda^2 \text{ is positive} \\ i\lambda r & \text{if } \lambda^2 \text{ is negative} \end{cases} \tag{2.11}$$

$$\frac{d^2R}{d\varepsilon^2} + \frac{1}{\varepsilon}\frac{dR}{d\varepsilon} + (1 - \frac{k^2}{\varepsilon^2})R = 0 \tag{2.12}$$

For this equation the solution is given by the Bessel functions. For $\varepsilon = \lambda r$ the solutions are the first and second kind Bessel functions $J_{\mathrm{k}}(\lambda r)$ and $Y_{\mathrm{k}}(\lambda r)$. For $\varepsilon = i\lambda r$ the solutions are the first and second kind modified Bessel functions $I_{\mathrm{k}}(\lambda r)$ and $K_{\mathrm{k}}(r)$. The total solution is a superposition of these functions:

$$R = CJ_{\mathrm{k}}(\lambda r) + DI_{\mathrm{k}}(\lambda r) + EY_{\mathrm{k}}(\lambda r) + FK_{\mathrm{k}}(\lambda r) \tag{2.13}$$

The solution must be single valued in the center and can not have a singularity, therefore $E = F = 0$.

By applying boundery coditions $R(a) = 0$ and $\frac{dR}{dr}(a) = 0$ we find the system of equations:

$$\begin{bmatrix} J_{\mathrm{k}}(\lambda a) & I_{\mathrm{k}}(\lambda a) \\ \frac{dJ_{\mathrm{k}}}{dr}(\lambda a) & \frac{dI_{\mathrm{k}}}{dr}(\lambda a) \end{bmatrix} \begin{Bmatrix} C \\ D \end{Bmatrix} = 0 \tag{2.14}$$

If the determinant is set equal to zero, the following equation follows:

$$J_{\mathrm{k}}(\lambda a)\frac{dI_{\mathrm{k}}}{dr}(\lambda a) - \frac{dJ_{\mathrm{k}}}{dr}(\lambda a)I_{\mathrm{k}}(\lambda a) = 0 \tag{2.15}$$

When the roots of λa are evaluated and they are labeled with their mode numbers. [7] Here n represents the radial wavenumber and m the circumferential wavenumber. The shapes of the modi as corresponding to the wavenumbers are shown in figure 2.1.

m n	0	1	2	3
0	3.196	4.611	5.906	7.143
1	6.306	7.799	9.197	10.537
2	9.440	10.958	12.402	13.795
3	12.577	14.108	15.579	17.005

From equation 2.4 we find that:

$$\omega_{mn} = \frac{(\lambda a)^2_{mn}}{a^2}\sqrt{\frac{Ed^2}{12\rho(1-\nu^2)}} \tag{2.16}$$

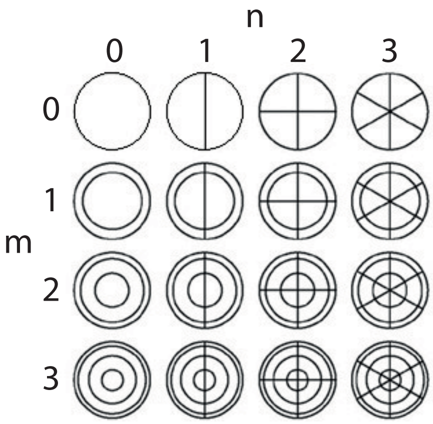

FIGURE 2.1: Different membrane modi sorted on wavenumbers m and n. [8]

2.2 Natural frequencies of an intrinsically stressed membrane

The behavior of an intrinsically stressed membrane is dominated by this tension. This can be seen from the relation 2.1. The tension is given by N and can be created by a stress introducing mechanism or is a result of the fabrication process.

The equation of motion for an intrinsically stressed membrane is: [7, 9]

$$-N\left(\frac{\delta^2 w(r,\theta,t)}{\delta r^2}+\frac{1}{r}\frac{\delta w(r,\theta,t)}{\delta r}+\frac{1}{r^2}\frac{\delta^2 w(r,\theta,t)}{\delta\theta^2}\right)+\rho d\omega\frac{\delta^2 w(r,\theta,t)}{\delta t^2}=0 \tag{2.17}$$

If we use 2.17 and make use of variation of variables we find:

$$\frac{r^2}{R}\frac{d^2R}{dr^2}+\frac{r}{R}\frac{dR}{dr}+r^2\frac{\omega^2\rho h}{N}=-\frac{1}{\Theta}\frac{d^2\Theta}{d\theta^2}=k^2 \tag{2.18}$$

This gives the separated equations 2.19 and 2.20.

$$\frac{d^2\Theta}{d\theta^2}+k^2\Theta=0 \tag{2.19}$$

$$r^2\frac{d^2R}{dr^2}+r\frac{dR}{dr}+\left(\frac{\omega^2\rho d}{N}r^2-k^2\right)R=0 \tag{2.20}$$

$$\Theta=A\sin(n\theta)+B\cos(n\theta) \tag{2.21}$$

$$\lambda^2=\frac{\omega^2\rho d}{N} \tag{2.22}$$

m n	0	1	2	3
0	2.404	5.520	8.654	11.792
1	3.832	7.016	10.173	13.323
2	5.135	8.417	11.620	14.796
3	6.379	9.760	13.017	16.224

Table 2.1: Values for $(\lambda a)_{\mathrm{mn}}$

$$\epsilon^2 = \lambda^2 r^2 \tag{2.23}$$

$$\frac{d^2R}{d\epsilon^2} + \frac{1}{\epsilon}\frac{dR}{d\epsilon} + \left(1 - \frac{n^2}{\epsilon^2}\right) R = 0 \tag{2.24}$$

Which is the Bessel's differential equation with solution:

$$R_n = C_k J_k(\epsilon) + D_k Y_k(\epsilon) \tag{2.25}$$

The solution of $Y_{\mathrm{k}}(0) = \infty$, which is impossible in the center of a membrane, therefore D_{k} must be 0.

The other condition is $w(a) = 0$, which gives $R(\epsilon) = J_{\mathrm{k}}(\lambda a) = 0$. Which results in values for $(\lambda a)_{\mathrm{mn}}$ as given in table 2.1. The m and n values represent the circumferential and radial wavenumber respectively.

From equation 2.22 and 2.23 we find:

$$\omega_{\mathrm{mn}} = \frac{(\lambda a)_{\mathrm{mn}}}{a}\sqrt{\frac{N}{\rho d}} \tag{2.26}$$

The difference in natural frequencies between both behaviors is shown in figure 2.2. The figure shows that the natural frequency lowers with increasing thickness for membrane behavior and for plate behavior increases with increasing thickness.

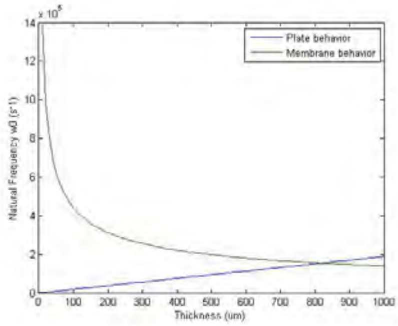

Figure 2.2: Natural frequencies of plate and membrane behavior under varying thickness. a = 0.24 cm, N = 10 000 N m^{-1}. Tension N is uniformely distributed, perpendicular to the rim applied.

2.3 Static deflection under constant uniform Pressure

The static deflection of the membrane can be used to evaluate the mechanical properties. Due to the fact that the membrane is in equilibrium, differences in the characteristics over area of the membrane can be evaluated. Therefore the measurements give information on the uniformity of the membrane, intrinsic stresses and bending stiffness.

According to Schomburg [10], when a static pressure is applied to the membrane, the membrane bends till a static equilibrium is reached. The shape of this membrane deflection depends on the thickness of the membrane compared to the magnitude of deflection. Typically when the magnitude of deflection is small compared to the thickness of this membrane plate behavior is observed, otherwise membrane behavior. The shape of the membrane is determined by the stiffness and the fact that the membrane is fixed at the rim. The shapes of both cases are given in equation 2.27 and 2.28, for membrane and plate behavior respectively.

$$w(r) = w_0 \left(1 - \frac{r^2}{a^2}\right) \tag{2.27}$$

$$w(r) = w_0 \left(1 - \frac{r^2}{a^2}\right)^2 \tag{2.28}$$

The vertical components of the forces on the membrane must be in equilibrium. Therefore we define two forces: $F_{\mathrm{s},z}$ and $F_{\mathrm{p},z}$, respectively the force acting on the membrane due to the support and the force applied by the pressure.

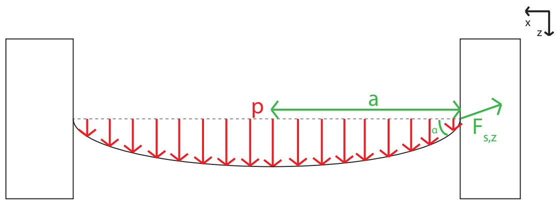

FIGURE 2.3: Membrane under constant uniform load.

$$F_{\mathrm{s},z} = 2\pi\sigma dasin(\alpha) \tag{2.29}$$

$$F_{\mathrm{p},z} = \Delta p \pi a^2 \tag{2.30}$$

For small deflections α the sine is approximately the same as the tangent, which equals the slope of the membrane at the rim. w_0 is described by the equation for membrane behavior (eq 2.27). When large loads are applied to the membrane this approximation can become inaccurate. Differentiating the expression for membrane behavior to r and solving with equations 2.29 and 2.30, gives expression 2.31.

$$\Delta p = \frac{4w_0 d}{a^2}\sigma \tag{2.31}$$

The total stress σ consists of two parts. The intrinsic stress in the membrane (σ_T) and the stress caused by the deflection of the membrane (σ_D). The stress caused by deflection can be calculated from the radial and tangential strain. The radial strain is assumed to be constant over the entire membrane. The radial ϵ_r and tangential strain ϵ_t are given by Hooke's law in equations 2.32 and 2.33 respectively. [10]

$$\epsilon_\mathrm{r} = \frac{1}{E}(\sigma_\mathrm{r} + \nu\sigma_\mathrm{t}) \tag{2.32}$$

$$\epsilon_\mathrm{t} = \frac{1}{E}(\sigma_\mathrm{t} + \nu\sigma_\mathrm{r}) \tag{2.33}$$

The length of the neutral line over the membrane is given by equation 2.34. From this expression the strain is given by eq 2.35. [7]

$$L \approx 2a(1 + \frac{2w_0^2}{3a^2} - \frac{2w_0^4}{5a^4}) \tag{2.34}$$

$$\epsilon_\mathrm{t} \approx \frac{2w_0^2}{3a^2} \tag{2.35}$$

When combining equations 2.32, 2.33 and 2.35, and we assume the tangential and radial strains to be equal, we find:

$$\sigma_\mathrm{r} = \epsilon_\mathrm{r}\frac{E}{1-\nu} = \frac{2w_0^2 E}{3a^2(1-\nu)} \tag{2.36}$$

Resulting in the total stress σ.

$$\sigma = \sigma_\mathrm{T} + \frac{2w_0^2 E}{3a^2(1-\nu)} \tag{2.37}$$

When we introduce this expression in equation 2.31, we find:

$$\Delta p = \frac{4w_0 d}{a^2}\left(\sigma_\mathrm{T} + \frac{2w_0^2 E}{3a^2(1-\nu)}\right) \tag{2.38}$$

2.4 Static deflection under central point loading

The expression for central point loading can is found in the same way. We take uniform load $F_{\mathrm{p},z}$ to be point load P and solve the expressions. We find equation 2.39.

$$P = 4\pi d w_0 \left(\sigma_{\mathrm{T}} + \frac{2w_0^2 E}{3a^2(1-\nu)} \right) \tag{2.39}$$

2.5 Conclusion

From the expressions for the characteristics of a membrane it can be seen that intrinsic stress has a large influence on the type of behavior the membrane exhibits. In the design of a membrane this can be used to set the modes of the membrane to the frequencies of interest. Interesting is the fact that the natural frequency decreases with increasing thickness for membrane behavior and increases for plate behavior. Membranes used in sensors need to be limited in size. By making use of the characteristics of the two behaviors, smaller membranes can be build.

The difference in expressions for static and dynamic behavior of the membrane lead to possibilities to measure more material properties. By measuring the reactance to an applied frequency f, an additional parameter is introduced to solve the various material properties.

In the calculations uniformity of the membrane was used to solve the expressions. The uniformity of the designed membrane can be measured with the two variations of static measurements. Non-uniformity will cause differences in the measured deflection when changing the angle of the natural fiber.

Chapter 3

Design

The final behavior of the membrane is influenced by its design. The material and geometry posses parameters which determine the natural frequency of the membranes as described in chapter 2. Most material properties are still unknown and not documented in literature for materials printed on micrometer scale. The creation of 3D structures on micrometer scale by 3D printing, is hardly scientifically done or reported. Therefore approximations are made, which combined with the measurement methods are elaborated in this chapter.

3.1 Criteria

The goal is to design a few membranes and measure their characteristics. In chapter 2 the mathematical background of the predicted behavior is given. The goal of the experiments is to determine the different material properties on the scale at which the membranes are produced. Besides that, the influences of 3D printing on the geometry, characteristics and the uniformity of the produced membrane are investigated.

There are several parameters which have to be determined. These parameters are the Youngs modulus, the Poisson ratio and the intrinsic stress in the membrane. E, ν and σ_{T}. These parameters may vary for the different planes in which can be printed. These planes are the $x-y$, $x-z$ and $y-z$ planes.

3.1.1 Youngs Modulus

The Youngs Modulus can be measured in different ways. The first way is to measure the different modi of the membrane, when it exhibits plate behavior. In that case the bending stiffness of the plate is larger than the tension on the membrane. Therefore the frequency of the resonance is dependent on the Bending Stiffness D, which depends on the Young's Modulus. The bending stiffness is defined in equation 3.1.

$$D = \frac{Ed^3}{12(1-\nu^2)} \tag{3.1}$$

$$E = \frac{12\omega_{\mathrm{mn}}^2 a^4 \rho(1-\nu^2)}{d^2(\lambda a)_{\mathrm{mn}}^4} \tag{3.2}$$

When a static pressure is applied to the membrane, when it acts as a membrane, the displacement w_0 is a reference for the Youngs Modulus of the material. This can be done both by applying a static pressure (eq. 3.3) as well as a point pressure (eq. 3.4). The intrinsic stress on the membrane must be known to determine the Youngs modulus.

$$E = \frac{3\,(1-\nu)}{2w_0^2}\left(a^2\Delta p - 4\sigma_{\mathrm{T}} w_0 d\right) \tag{3.3}$$

$$E = \frac{3a^2(1-\nu)}{2w_0^2}\left(\frac{3P}{4\pi d a w_0} - \sigma_{\mathrm{T}}\right) \tag{3.4}$$

A beam which is only supported at one side will act as a free cantilever. The cantilever can expand freely and therefore stress or strain can not exist in the length direction. When no intrinsic stress occurs in a beam, the behavior of the beam will be dominated by the bending stiffness of the beam. From this the resonance frequency can be calculated and the Young's modulus can be found.

$$\omega = 1.875^2\sqrt{\frac{Ed^2}{12\rho L^4}} \tag{3.5}$$

Giving:

$$E = \frac{12\rho\omega^2 L^4}{1.875^4 d^2} \tag{3.6}$$

Equation 3.2 depends on material properties for which only educated queses can be made with the available literature. Equation 3.3 depends on the unknown variable σ_{T}, therefore 3.6 is used to determine the Youngs Modulus of the material. The effective Youngs Modulus can be different in the different planes of the printed structure. With cantilevers in different planes the effective Youngs Modulus can be measured.

3.1.2 Poisson's ratio

Poisson's ratio can influence the dynamic behavior of the system slightly. The significance of that deviation is relatively low, due to the fact that its value lies between 0 and 0.5 and is squared.

The Poisson's ratio is calculated via the dynamic plate behavior and the static deflection of the system.

$$\nu_{\mathrm{d}} = \sqrt{1 - \frac{Ed^2(\lambda a)^4_{\mathrm{mn}}}{12\rho\omega^2_{\mathrm{mn}}a^4}} \tag{3.7}$$

$$\nu_{\mathrm{s}} = 1 - \frac{2Ew_0^2}{3\left(a^2\Delta p - 4\sigma_{\mathrm{T}}w_0 d\right)} \tag{3.8}$$

3.1.3 Tension

The parameter of which the least literature is available is the tension. The tension determines if the membrane exhibits plate of membrane behavior. Therefore the tension is an important design parameter. The designed membranes will be used to determine the amount of tension that occurs in the printed part. Tension in the membranes comes from intrinsic stresses. These stresses can come from deformations during the print process or from thermal loading.

The tension can be measured when it is significantly larger than the bending stiffness. When we measure the frequency of an intrinsic stressed membrane we can derive the tension on the membrane from:

$$N = \rho d \left(\frac{a\omega_{\mathrm{mn}}}{(\lambda a)_{\mathrm{mn}}}\right)^2 \tag{3.9}$$

When the membrane is statically loaded with force the displacement is a measurement for the stress in the membrane:

$$\sigma_{\mathrm{T}} = \frac{a^2\Delta p}{4d\omega_0} - \frac{E\omega_0}{6d(1-\nu)} \tag{3.10}$$

3.2 Error Analysis

For membranes created on the micrometer scale it is important to know the error margins in the final result. The printer has many inaccuracies, like the accuracy in $x-y$ plane, layer thickness, STL rendering and material properties. These can lead to error margins larger than the distances created and measured.

The error found when calculating the natural frequency of the plate using equation 2.16 is given in equation 3.11.

$$\frac{\Delta w_0}{w_0} = \left(\left(2\frac{\Delta a}{a}\right)^2 + \left(\frac{1}{2}\left(\left(\frac{\Delta E}{E}\right)^2 + \left(\frac{\Delta\rho}{\rho}\right)^2\right)^{\frac{1}{2}}\right)^2\right)^{\frac{1}{2}} \tag{3.11}$$

The error found when calculating the natural frequency of the membrane using equation 2.26 is given in equation 3.12.

FIGURE 3.1: The processing steps from computer CAD design to 3D printed object.

$$\frac{\Delta w_0}{w_0} = \left(\left(\frac{\Delta a}{a}\right)^2 + \left(\frac{1}{2}\frac{\Delta rho}{rho}\right)^2\right)^{\frac{1}{2}} \tag{3.12}$$

3.3 STL file

3D printers are unable to interpret SolidWorks [11] data directly. Conversion of the model data to the 3D printer requires a workflow as depicted in figure 3.1. The current standard for model files in 3D printing is the STL format. This Standard Transform Language file consists of triangles which describe the geometry of the model. The triangulation consists of two phases. First the curved edges are split until they can be approximated by straight lines. Then the faces are triangulated. When the triangles have a narrow base instead of having a more equilateral form, inaccuracies arise during the recreation of the model. The printer translates the STL file back into a full geometry by matching the locations of the triangle points and add lines between these points. To recreate the model the contour generator uses a tolerance to match the location points. The base of the triangle must be larger than that of the tolerance of the contour generator in order to avoid that triangles are interpreted as being points lying at the same position. [12]

For membrane making with 3D print technology this is an important asset. The tolerances which are used during the conversion of the model to the STL file can be given as input in Solidworks. When lower tolerances are used than the tolerances used by the printer serious misalignment will cause deviations in the membranes. The models design are imported in SolidWorks to ensure there were no missing triangles in the process and the finest settings were used to create the finest mesh still distinguishable for the contour generator.

3.4 Structures

3.4.1 Support Structures

The different membranes and designed geometries must be supported in a larger structure. These structures are boxes as shown in figure 3.2. Three boxes are designed to support the membranes. Box 1 has a volume of $3\,\text{cm}^3$ and boxes 2 and 3 a volume of $1\,\text{cm}^3$. The boxes all have three planes, on which the strainsensors, membranes and cantilevers are placed. The strainsensors and cantilevers will be introduced in the coming sections. The size of the boxes is limited by the maximum measurement size of the Laser Vibro Meter and the increasing inaccuracies of the printer. The accuracy of the printer decreases when the volume of the box increases. Box 1 consists of 2 membranes, 3 strain-sensors and 3 cantilevers. Box 2 consists of 6 membranes

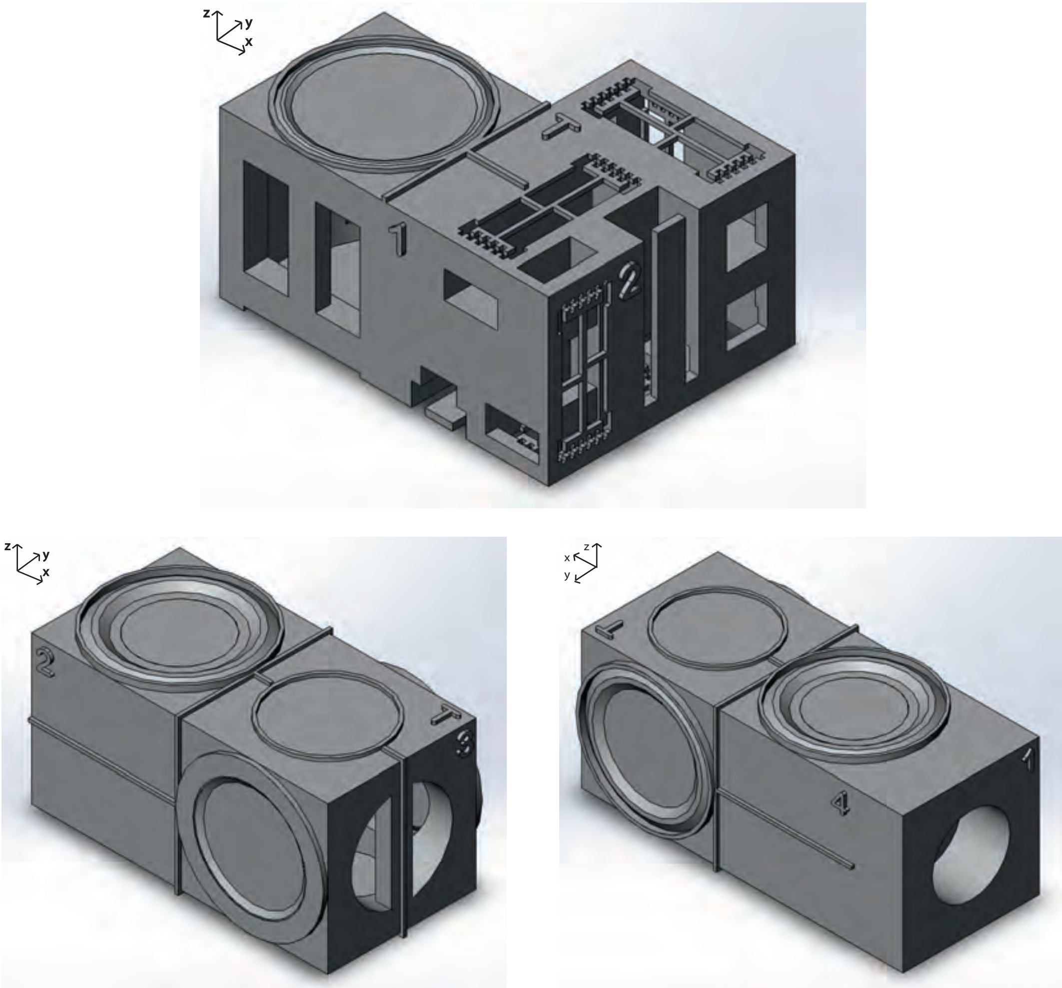

FIGURE 3.2: The three designed boxes sorted on order of number.

and box 3 of 7 membranes. Box 3 is a reinforced version of box 2, specially designed for static loading. The cavity is later tapped with 5 mm screw-thread to create an air tight connection to load the box with a static pressure.

3.4.2 Strain Sensor

Stress in the structure due to deformations can be found from measuring the strain in the structure. The strain in the sensor is measured in beams which are free to extend or shrink. By the deformation ΔL in the beam the strain can be calculated. The geometry given in figure 3.3 rotates around point O. The strain and resulting stress are given in equation 3.13 and 3.14 respectively.

$$\epsilon = \frac{ua}{bL} \tag{3.13}$$

$$\sigma_{\text{ii}} = \frac{Eua}{bL(1+\nu)} \left(\epsilon_{\text{ii}} + \frac{\nu}{1-2\nu} \left(\epsilon_{11} + \epsilon_{22} + \epsilon_{33} \right) \right) \tag{3.14}$$

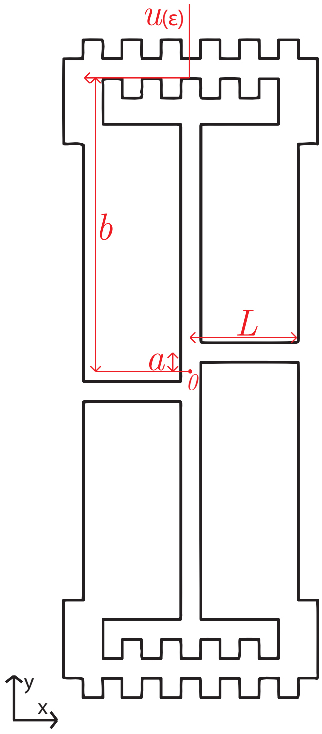

FIGURE 3.3: Strain sensor design

a	150 μm
b	3.800 μm
L	1.500 μm
$\mathbf{\frac{a}{bL}}$	26.31 m^{-1}

TABLE 3.1: Values used for strainsensor.

The sensors are placed at the three planes, with which the deformation in the structure can be measured. The measurement precision is highly dependent on the accuracy of the printer. Deformations of 1% need to be measurable. The accuracy of a typical printer is 100 μm. This accuracy is the minimum of u. Therefore factor $\frac{a}{bL}$ must be larger than 100. In this case the minimum deformation of 1% is measurable. When the factor is smaller, smaller deformations can be measured.

The used dimensions are given in 3.1. With this configuration a minimum strain of 0.2631% is measurable.

Error Analysis

The error in the measurements is very important due to the relatively low accuracy of the printer. The error in the strain and stress are given in equations 3.15 and 3.16.

$$\frac{\Delta\epsilon}{\epsilon} = \sqrt{\left(\frac{\Delta u}{u}\right)^2 + \left(\frac{\Delta a}{a}\right)^2 + \left(\frac{\Delta b}{b}\right)^2 + \left(\frac{\Delta L}{L}\right)^2} \tag{3.15}$$

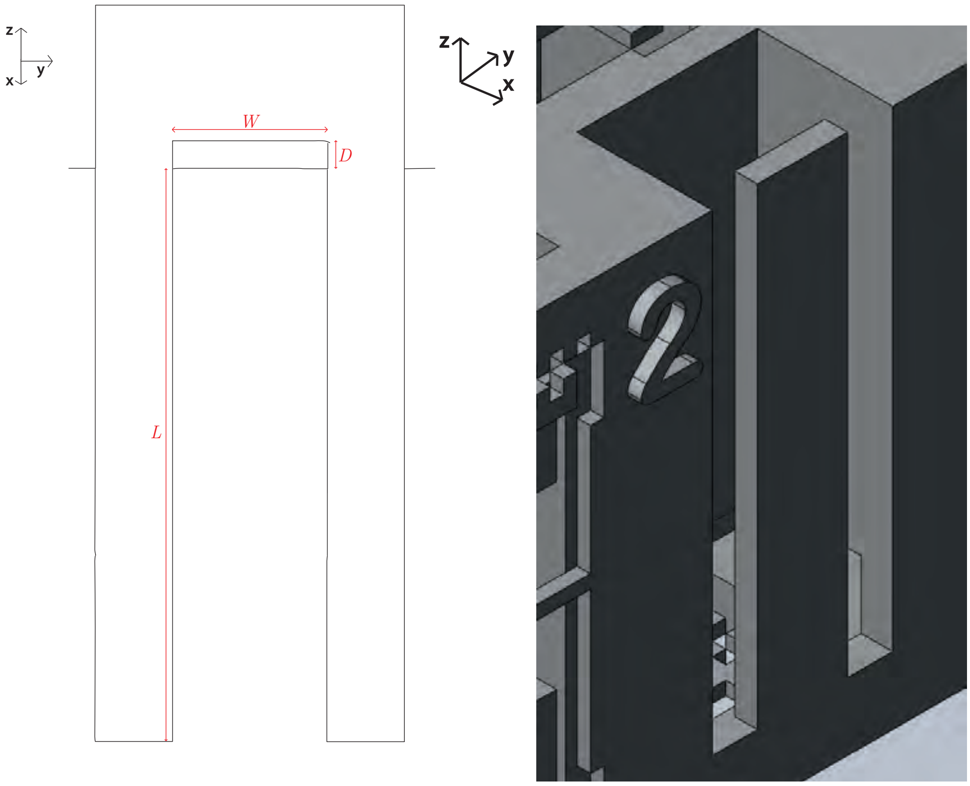

FIGURE 3.4: Cantilever Design in 3D

L	10.500 μm
W	2.000 μm
D	500 μm
ω_0	6.707 Hz

TABLE 3.2: Values used for cantilever

$$\frac{\Delta\sigma_{\text{ii}}}{\sigma_{\text{ii}}} = \sqrt{\left(\frac{\Delta E}{E}\right)^2 + \left(\frac{\Delta\nu}{\nu}\right)^2 + \left(\frac{\Delta\epsilon_{\text{ii}}}{\epsilon_{\text{ii}}}\right)^2 + \left(2\frac{\Delta\nu}{\nu}\right)^2 + \left(\frac{\Delta\nu}{\nu}\right)^2 + \left(\frac{\Delta\epsilon_{11} + \Delta\epsilon_{22} + \Delta\epsilon_{33}}{\epsilon_{11} + \epsilon_{22} + \epsilon_{33}}\right)^2} \tag{3.16}$$

3.4.3 Cantilever

The cantilever is used to determine the Youngs modulus of the structure. This is done by using equation 3.6. The cantilever design is shown in figure 3.4. The cantilever has room behind the beam to make cleaning easier and allow the beam to swing. The dimensions of the cantilever are given in table 3.2.

Error Analysis

The error in the Youngs modulus is given in equation 3.17.

$$\frac{\Delta E}{E} = \left(\left(\frac{\Delta\rho}{\rho}\right)^2 + \left(2\frac{\Delta\omega}{\omega}\right)^2 + \left(4\frac{\Delta L}{L}\right)^2 + \left(2\frac{\Delta d}{d}\right)^2\right)^{\frac{1}{2}} \tag{3.17}$$

3.4.4 Membranes

The membranes are thin circular plates that are supported by the box. This box must be stiff enough to withstand stresses introduced by the membrane when deflected. The stress of some structures is released by stress release mechanisms. A graphical representation of these structures on the support structure is shown in figure 3.2. The diameter of all membranes is 9.63 cm. The geometrical properties of the membranes are given in table 3.3.

Box	Zijde	Thickness (d) (μm)	Plane	Stress Release
1	T	64	x,y	Yes
1	D	64	x,y	No
2,3	D	16	x,y	Yes
2,3	D	16	x,y	No
2,3	T	144	x,y	Yes
2,3	T	144	x,y	No
2,3	2	112	x,z	Yes
2,3	4	144	x,z	Yes
3	3	64	y,z	No

Table 3.3: Geometrical properties of membranes with diameter 9.63 cm.

3.4.4.1 Stress Release Mechanism

As discussed earlier the membrane can be stressed. These can come from deformations and material properties. Membranes will rupture when the stresses are to large. Therefore stress releases are designed to release intrinsic stresses. Membranes with and without stress releases are designed to compare the influence of the stress. The stress release mechanism consists of a wrinkle around the membrane which can extend to release the stress. The difference between the stress-released and stressed membranes is shown in Figure 3.5. The design of the mechanism is simple, to avoid problems with the printing thickness of the walls. The minimum width in the $x - y$ direction is kept at a minimum of 100 μm. This width defines the angle of the release mechanism. The height of the model is equal for both the membrane and the stress release mechanisms.

Figure 3.5: Difference with and without stressrelease

3.5 Conclusion

The different expressions for the characteristics of a vibrating or loaded plate are used to design a vibrating membrane. Many of these material properties are still not documented in literature on micrometer scale. With a few geometries and structures these material properties will be investigated.

Inaccuracies in the printing process can exceed the values of interest. Strain in a structure can be smaller than the deviation in this structure designed to measure the strain. Therefore these tolerances are taken into account during the design by creating larger measurement structures than the minimum print-sizes of the printer.

Intrinsic stress can rupture the membrane. With stress-release mechanisms this can be avoided. These structures can stretch over the radius of the membrane, lowering the stress on the membrane.

Chapter 4

Fabrication

4.1 Comparison different techniques

There are many commercially available techniques which can be used to 3D print a model. These different techniques have there consequences on the strength of the material and the dimensions which can be printed. The membrane must be small enough to be useful in applications and the material has to be stiff enough to withstand the applied pressures.

In table 4.1 the different material properties are shown as known in literature and the minimum dimensions which are possible to print with the technique. Some techniques use support material to support the printed parts of the model during fabrication. The choice for a printer is primarily made based on the dimensions which can be printed.

4.2 Suppliers

The initial idea was to outsource the printing of the membrane. External parties possess more knowledge on the after-production process and practical physical limitations of the printing process. Based on table 4.1, Materialize is chosen as supplier because they make use of the Polyjet technology. Polyjet technology creates models with high accuracy and thin layer-thicknesses. These features are critical to produce thin membranes with predictable characteristics.

Models were printed with the Objet Eden 250 from the chair Robotics and Mechatronics. This printer was used to lower production times due to the in house production. The Objet Eden 250 uses PolyJet technology but is an older version of the Objet Eden 500 used at Materialise. The printer at Robotics and Mechatronics only prints Fullcure model material, Materialise also prints VeroWhite model material.

Technique	Machine	Company	Layerthickness (μm)	**x,y Plane Resolution** (μm)	Youngs Modulus MPa	Tensile Strength MPa	Poisson's Ratio	Density $\mathrm{kg\,m^{-3}}$
Selective Laser Sintering	EOS Formiga P100	3d Print Company	100	56	1,700	48 [13]		
Metal FDM	Concept Laser M3	3d Print Company	20-80		200,000	570 [13]		
Fused Deposition Modeling	Leapfrog Xeed		10	350	2,415 - 2,622	24 - 59 [14]	0.35	1070 [15]
Fused Deposition Modeling	Leapfrog Creatr	3D Print Zeeland	50	350	2,415 -2,622	24 - 59	0.35	1070
Fused Deposition Modeling	Ultimaker 2		20	400				
PolyJet	Objet Eden	Materialise	16	200	2495 [16]	49.8	0.33	1175
Stereolithography		Materialise	100	200	2655 -2880	63.1 - 74.16		
Fused Deposition Modeling		Shapeways	200	200				

Table 4.1: Different Techniques

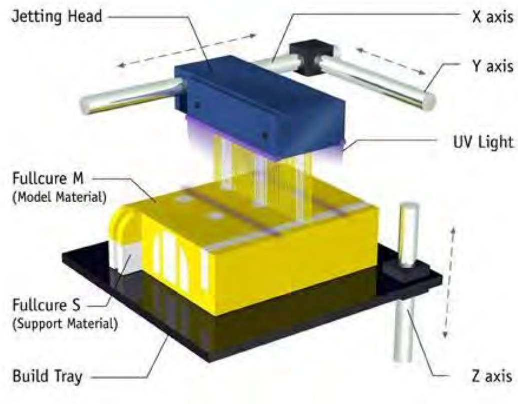

FIGURE 4.1: PolyJet printing process [17]

4.3 PolyJet Technology

The PolyJet technology of Stratasys, jets photosensitive polymer material on a plate. The printer head has two jetting mechanisms. One for the material itself, and one for the support material. The materials are jetted on the plate with a layerthickness of 16 or 32 μm. The layerthickness depends on the modus of the printer. Simultaneously with the jetting the material is cured by Ultra-Violet light. The plate lowers as much as the layerthickness and a new layer is applied. The support material can be removed by hand or with water jetting.

In September a new type of printer is launched in the Eden Series, the 260VS. This printer makes use of support that is fully soluble which makes cleaning by waterjetting unnecessary. This printer has promising specifications which make the printer a logical choice for the research in this report. Complex geometries can be produced due to the water soluble support material. The support material is used to support the overhanging and complex shapes of the model without adding stresses to the material. Unfortunately the printer has not been delivered in Europe yet. Therefore it was not possible to use the printer to produce models within the time frame of this research.

4.4 Conclusion

3D printing is a technique which can be used to create many types of models. The technique evolves and with this thinner structures can be created. Momentarily most printing techniques are designed to create centimeter scale models with smooth appearances. By using PolyJet technology this boundary can be extended to micrometer scale structures. The printer is able to print on this scale, but the removal of support material is challenging. For the removal of the support a new cleaning method needs to be designed.

Chapter 5

Cleaning Process

The cleaning process is the most difficult step of the fabrication process. The advised method to clean the structure is by waterjetting. With the fragile components in the structure, this method is not applicable for thin membranes. The cleaning will be done in house, to avoid breaking the structure. To release the structure from its support a new way of support removal has to be found.

5.1 Dissolution

To separate the support material and the structural material from each other, the materials can be dissolved in a solvent. Crucial for this process is that the time needed to dissolve the structural material is much larger than the time needed for the support material to dissolve. This is the case when the solubility of structural material is much smaller than that of the support material. Another possibility is to have a lower saturation concentration for the structural material.

During dissolution molecules of material release from the main structure. These diffuse through the boundary layer to the bulk solvent. In this boundary layer the concentration decreases from the saturation concentration to the bulk concentration. The amount of material dissolved can be calculated using the Noyes-Whitney equation: [18, 19]

$$\frac{dm(t)}{dt} = A(t)\frac{D}{d}\left(C_{\mathrm{s}} - C_{\mathrm{b}}(t)\right) \tag{5.1}$$

The dissolution is limited by the diffusion of dissolved material through the boundary layer. At the material/solvent interface the material dissolves with the maximum saturation concentration (C_{s}). Dissolved material will diffuse away from the material to lower concentrations until it reaches a stationary concentration. This concentration is defined as the bulk concentration (C_{b}). The boundary layer (d) defines the path length needed to reach the bulk concentration. The dissolution constant (D) is given by the mass flux per unit area over the concentration gradient in the boundary layer (equation 5.2)[20]. When the dissolution constant is multiplied

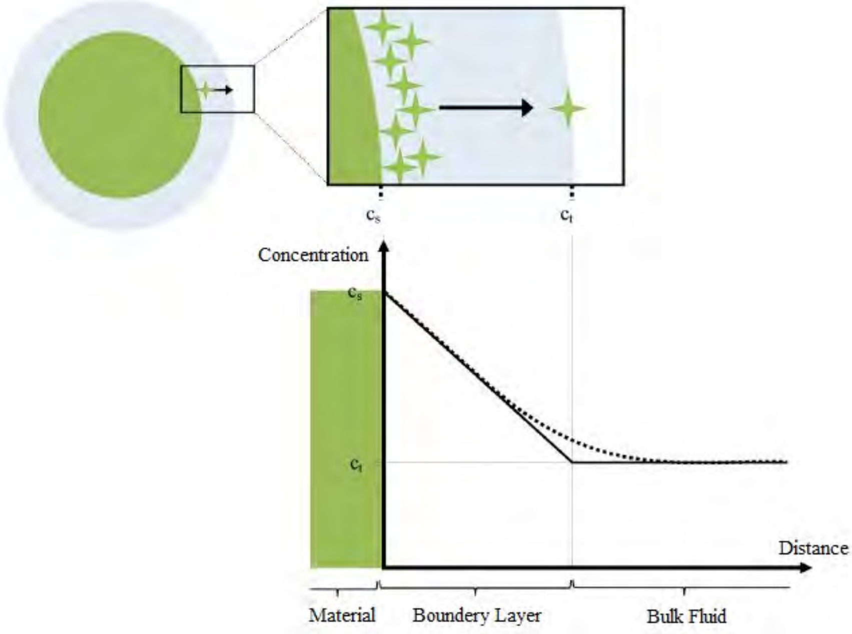

FIGURE 5.1: Concentration gradient between material/solvent interface and bulk fluid. [18]

with the area (A) available for dissolution and the concentration gradient, the mass change rate is found. The diffusion of material is given by figure 5.1.

$$J = -D\frac{\delta\phi}{\delta x} \tag{5.2}$$

The diffusion coefficient over the boundary layer thickness is constant for a fixed geometry. This constant is defined as dissolution rate constant (k) in equation 5.3. This bulk concentration is given by the amount of material that left the structure. This concentration is therefore given by the mass difference between $t = 0$ and t over the volume of the solvent as shown in equation 5.4. In this equation (V_m) represents the volume of the material and (V_s) the volume of the solvent.

$$k = \frac{D}{d} \tag{5.3}$$

$$C_\mathrm{b} = \rho\frac{V_\mathrm{m}(0) - V_\mathrm{m}(t)}{V_\mathrm{s}} \tag{5.4}$$

5.2 Geometries

The saturation concentration C_s is dependent on the material and solvent used, independent on the geometry. The dissolution rate constant k is dependent on the geometry due to the differences in boundary layers. Also the ratio between surface area and volume of the structure has influence on the total mass change rate. Therefore different geometries are examined with respect to their influence on the rate of mass change.

Plate A plate dissolving in a bath with a volume V_s is fixed to the bottom of the bath. The solvent can access only one side of the plate. Dissolving at the sides of the plate is assumed to be negligible. Because the width and length of the plate are much larger than the thickness of the plate. Therefore the area of the plate is assumed to be mass change 1rate determining. This leads to differential equation 5.5 with the solution for h given in equation 5.6. In the case used in chapter 6, where both sides can dissolve, a factor 2 needs to be added.

$$\frac{dh(t)}{dt} = k\left(\frac{lw\left(h(0) - h(t)\right)}{V_\mathrm{s}} - \frac{C_\mathrm{s}}{\rho}\right) \tag{5.5}$$

$$h(t) = h(0) + \frac{C_\mathrm{s}V_\mathrm{s}}{wl\rho}\left(e^{-\frac{wlkt}{V_\mathrm{s}}} - 1\right) \tag{5.6}$$

Box The box is defined by its width, length and height (w, l and h). The dissolving process on all planes is assumed to be uniform, due to homogeneous diffusion. For this purpose a running variable x is introduced, resulting in differential equation 5.10.

$$l(t) = l(0) - 2x(t) \tag{5.7}$$

$$w(t) = w(0) - 2x(t) \tag{5.8}$$

$$h(t) = h(0) - 2x(t) \tag{5.9}$$

$$\frac{dx(t)}{dt} = \frac{2k}{V_\mathrm{s}}\left(\frac{C_\mathrm{s}V_\mathrm{s}}{\rho} - 2\left(h_0 l_0 + w_0\left(h_0 + l_0\right)\right)x(t) + 4\left(w_0 + h_0 + l_0\right)x(t)^2 - 8x(t)^3\right) \tag{5.10}$$

Sphere A uniform sphere is dissolved in the bath. The dissolution will decrease the radius of the sphere, resulting in the differential equation 5.11 and solution 5.12.

$$\frac{dr(t)}{dt} = 4k\left(\frac{C_\mathrm{s}}{\rho} - \frac{4\pi r_0^2}{3V_\mathrm{s}} + \frac{4\pi}{V_\mathrm{s}}r(t)^2\right) \tag{5.11}$$

$$r(t) = \frac{\sqrt{3C_\mathrm{s}V_\mathrm{s} - 4\pi\rho r_0^2}\tan\left(\frac{8kt\sqrt{\pi C_\mathrm{s}V_\mathrm{s} - \frac{4}{3}\pi^2\rho r_0^2}}{\sqrt{\rho}V_\mathrm{s}} + \tan^{-1}\left(\frac{2\sqrt{3\pi}\sqrt{\rho}r_0}{\sqrt{3C_\mathrm{s}V_\mathrm{s} - 4\pi\rho r_0^2}}\right)\right)}{2\sqrt{3\pi}\sqrt{\rho}} \tag{5.12}$$

Cylinder A cylinder with a certain height and radius is dissolved. The dissolution in radius is assumed to be dominant over the change of height of the structure. This results in differential equation 5.13.

$$\frac{dr(t)}{dt} = -k\left(r(t)+h\right)\left(\frac{C_\mathrm{s}}{\rho} - \frac{h\pi\left(r_0^2 - r(t)^2\right)}{V_\mathrm{s}}\right) \tag{5.13}$$

5.3 Vaporization

During the process of dissolving the support material, the solvent can evaporate. Especially volatile solvents like ethanol have to be handled with care. When too much solvent evaporates, the bulk concentration rises. Resulting in a lower dissolving rate.

The vaporization rate of a solvent is given by equation 5.14. [21] As can be seen the vaporization rate can be lowered by various variables. These variables are the area of the solvent/air surface and the solvents pressure in the surrounding. Therefore the solvent container must be sealed to create a vaporization equilibrium in the container and stop continuous evaporation.

$$\frac{dm}{dt} = A\left(P_\mathrm{v} - P\right)\sqrt{\frac{mw}{2\pi RT}} \tag{5.14}$$

5.4 Solubility

The chemical compositions of the support material and model material are used to determine a suitable solvent for dissolving the support material. Fullcure 705 and fullcure 720 are used as support and model material respectively. Fullcure 705 consists of Polyethylene Glycol, 1,2-Propylene Glycol, Acrylic Monomer, Glycerin and Photoinitiator. Fullcure 720 consists of Isobornyl Acrylate, Acrylic Monomer, Acrylate Oligomer and Photoinitiator. The solubility of these different materials can be found in table 5.1.

	705	720	Water	Ethanol	THF	Acetone	Chloroform	TCB	ODCB
Isobornyl Acrylate [22]		10-30%	0	0	+	0	0	0	0
Polyethylene Glycol [23]	20-50%		+	+	+	+	+	0	0
1,2-Propylene Glycol [23]	20-50%		+	+	+	+	+	0	0
Glycerin [22]	10-30%		+	0	+	0	0	+	+

TABLE 5.1: Solubility of components of FullCure 705 and 720.

The different solvents are tested for their abilities to solve the materials. An ultrasonic bath filled with water will be used to investigate the impact of the vibrating water on the support material. Still water will be used as comparison. The chemicals Ethanol, Acetone and Potassium hydroxide will be tested as a result of the known solubilities. Potassium hydroxide is a solvent used by fellow home users, and therefore will be tested on its solubility. [24, 25]

5.5 Design

The mathematical models for the geometries are tested with several structures. These structures provide information on the limits in which the presented cleaning method can be used.

Cube The cube is a relatively simple geometry to evaluated. The planes of the cube are known, and the influence on the corners can be investigated. A cube of $1\,\mathrm{cm}^3$ is used to find the dissolving rate of the support material on the different planes of the cube. The cube has 4 convex corners, giving information on the influence of the solvent on strongly curved positions. The second cube has a concave corner, created by removing a $0.25\,\mathrm{cm}^3$ cube from a $1\,\mathrm{cm}^3$ cube. This way the impact of the solvent for releasing a concave cavity is investigated. Both cubes are shown in figure 5.2. The boxes have little reference points on the planes, to determine the amount of model material dissolved. The points are little cubes with a size of $500 \times 500 \times 500\,\mu\mathrm{m}$, bigger than the accuracy of the printer. The points are used as references to determine the dissolved amount of material. Besides the solubility of the model material the dissolution of the support material is measured. To ensure the printer prints support material at all sides of interest an additional plane is added on top with a thickness of $16\,\mu\mathrm{m}$. Now the support material will be printed at all sides and the dissolving process can be investigated for all planes of the cube.

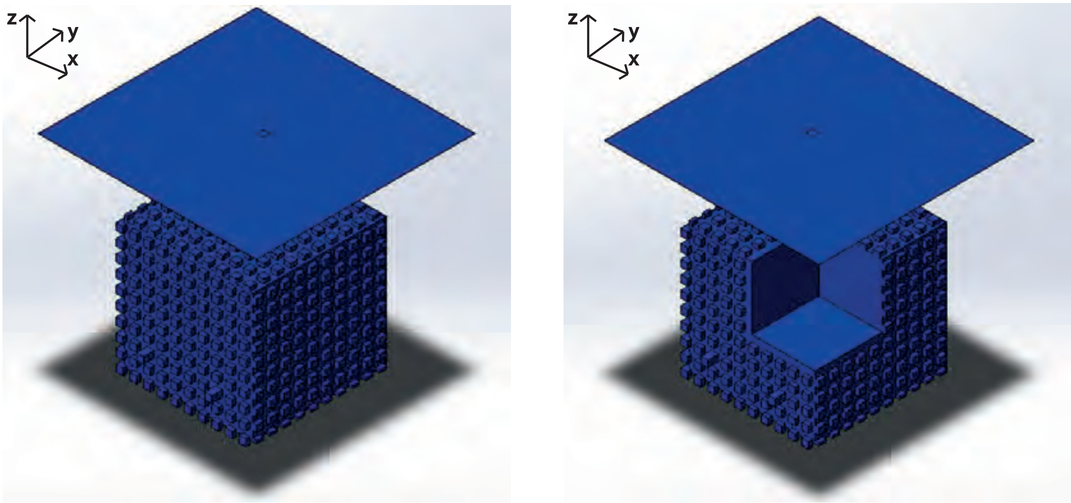

FIGURE 5.2: Cubes used for determining dissolving parameters.

Cylinder During the dissolution the radius of the cylinder decreases. Therefore the available area for dissolution decreases quadratically. The decrease in surface area will slow the dissolving process and therefore can be a design tool to build membranes. Also differences in dissolution rates between the $x-z$ and $y-z$ planes can be found. The cylinders are shown in figure 5.3. Both cylinders have a small cavity to show their orientation. The cylinder for 705 has a cylindrical plate on top to ensure the support material is printed cylindrical around the model.

Cavity Support material printed inside small cavities or canals is the most difficult to remove. When producing membranes or other complex micro scale structures, they have to be supported and will be in at a non-surface location. This means that material in the cavity must be released. A few different canals are produced to see the influence of different geometries on the dissolution rate in these spaces. The canals are shown in figure 5.4. In the figure the angles between the walls and shapes of the canals are shown1.

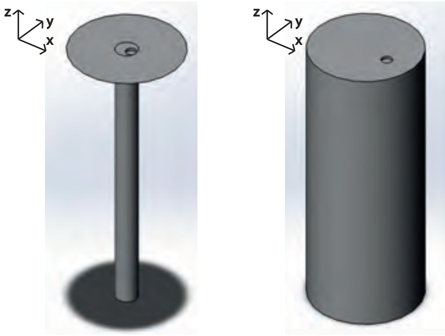

FIGURE 5.3: Cylinders used for determining dissolving parameters. Left for support material, right for model material.

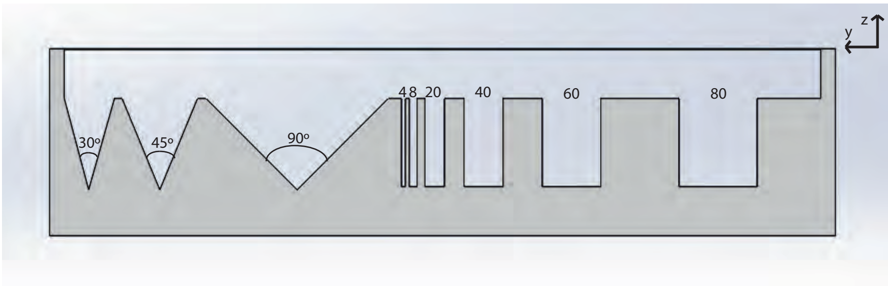

FIGURE 5.4: Plate with canals. The width of the canals is given in hundreds of micrometers.

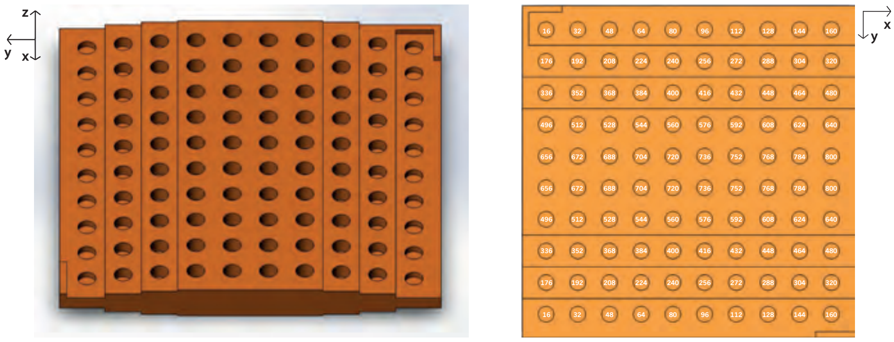

FIGURE 5.5: Plate with membranes to dissolve. Left the membranes as orientated in the plate with their thickness in μm.

Membrane plate Two geometries are most influential on the dissolution process during membrane fabrication. These two geometries are the plate and the cylindrical cavity. Measurements on their solubilities are done by dissolving a plate filled with membranes. These membranes have their own thicknesses and can be used to determine the influence of the solvent on to-be-released membranes. The sizes of the membranes are given in figure 5.5, the height of the plate varies with the thickness of the membranes lying in the plane. In order of thickness these thicknesses are, 400 μm, 700 μm, 900 μm and 1000 μm. Small thickened lines are placed on the upper-left and lower-right corner to determine the orientation of the plate when printed. The structure will be filled equally with support material. First the model will solve as a plate. Second, when the support material surrounding the model is dissolved, solvent can enter the cavities and dissolution rates within these cavities can be measured.

5.6 Conclusion

Currently used cleaning methods can not be used to rinse small scale models. The models will be harmed due to the impact of the forces. By using dissolution the support material can be released from the model material in a controlled way. The time needed to dissolve a model is dependent on the geometry. Geometries have their own boundary layer length and ratio between volume and surface area. These two influence the dissolution time. The different geometries designed will give insight in these dissolution times, which can be used as a design tool to rinse complex models.

Chapter 6

Measurements

In this chapter the different measurements are elaborated which are earlier designed in this report to measure the characteristics of the membranes produced. The results are shortly discussed and more general conclusions are made in a later chapter.

6.1 Procedure

A few phases were designed to measure the characteristics of the membrane. These phases are numbered one till four. Over time the conclusion had to be made that an additional phase had to be added to the research. This phase is called phase zero and contains the measurements on dissolving the support material. Without this phase the fabrication of membranes would be impossible. Due to this extra phase, some later phases where not totally completed in the time frame of this report. For the sake of information archiving and clarity an overview of the different phases is given in this section. In table 6.1 the progress of the different phases is given.

Phase 1	Strain sensor	Not completed
	Optical Microscope	Partly completed
	WLIM	Completed
Phase 2		Not completed
Phase 3		Completed
Phase 4		Completed

TABLE 6.1: Phases as performed during the research.

Phase 0 - Dissolution

The different geometries are soaked in a bath with different solvent. First the influence of an ultrasonically excited solvent is examined. Second different solvents are used to determine the most suitable one. With this solvent the last step of dissolving the geometries is performed.

Phase 1 - Reference Measurements

The first phase consists of measurements which give fast and clear results. These results can be used during other experiments. For example the strainsensors give insight in the stress of the material, which is useful information when measurements on the membrane are performed.

Strain sensor The measurements are done using the optical microscope. The microscope takes a digital picture which analyzed using the computer. The phase difference between the structure and the sensor is used to determine the displacement $u(\epsilon)$.

Microscopic Research It is possible that stress deforms the structure in various ways. Therefore research on the appearance of the structure and the membranes/components is done. This research consists of measuring the diameter of the membranes, the angle between the different planes of the model and visual inspection on the different parts produced.

White Light Interferometry The White Light Interferometric Microscope is used to determine the curvature of the membranes. It can happen that due to stresses and deformations during the production process the membranes are not spanned flat in their supports. The height profile of the membrane is measured without any applied forces.

The White Light Interferometric Microscope shines white light on the object and measures the path length of the measurement and the reference beam. The pathlength of the measurement beam is changed, and compared relative to the reference beam. When they are equal a maximum modulation due to interference is observed. This maximum value means that the z-value of the positioning stage equals the z-value of the objects height. [26]

Phase 2 - Dynamic Measurements

The membrane is designed to resonate at predetermined frequencies. When these modes are analyzed a part of the local spectrum can be regenerated. The modes of the membrane are measured during this phase.

The dynamic behavior is measured by exciting the membranes with a speaker. This speaker is used to produce different frequencies and the deflection $w(r, \theta, f)$ of the membrane is measured. When the modes are found by applying the corresponding frequency, this can be used. More likely is the case that the deflection is a superposition of several natural modes. Proper orthogonal mode decomposition [27] is used to find from $w(r, \theta, f)$ the natural modes. A technique which makes use from the fact that each harmonic movement of the membrane must be a superposition of natural modes.

The cantilever is measured in the same way as the membranes. The measurements are done every week to investigate the change in material properties over time.

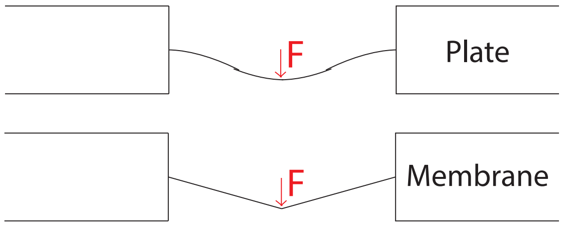

FIGURE 6.1: Plate shape versus membrane shape under static loading.

Phase 3 - Static Measurements

The system can be excited statically by applying a force on the membrane. Measurements on the deflection of the membrane are done by making use of the WLIM. The bending can be non-uniform over the radial and angular position of the membrane. The deflections at the radial and tangential positions on the membrane give insight in the uniformity.

Box 3 is designed to withstand the forces acting on the structure when the box is pressurized. Regulated by a valve Nitrogen is added to the chamber. By slowly increasing the pressure the bending for these pressures can be found.

Static measurements can also be performed with a static point load. The bending shape of the membrane gives information on the type of behavior the membrane exhibits. The different bending shapes are shown in figure 6.1. By using the equations as derived in chapter 2 the material properties can be determined.

Phase 4 - Destructive measurements

When other phases are done, the structures are sacrificed to obtain information on the geometric influence of the printing process. Membranes are cut in two pieces to investigate the binding of layers in the z-direction. Geometric information on stress release mechanisms can be obtained and examined.

The destruction of the membranes is done with a lancet to create a small cut and minimize physical influence of the cutting on the membrane.

6.2 Cleaning Process

6.2.1 Measurement setup

The weight and size of the model and support material are measured. The changes in weight and size of the material are a measurement for the dissolving rate of the material. It appeared that the support material dissolves in little flakes consisting of separated layers. These flakes float in the solvent, which make it harder to measure the total volume of the material. These flakes of material are considered to be completely dissolved.

The size of the material is measured by timelapsing the dissolving process. Two cameras capture once per 1.5 or 5 minutes a picture of the models in the solvent. The positions of these cameras are chosen in such a way that the plane of interest for the specific geometry is captured. In figure 6.2 the measurement setup is shown. The models soak in the bath placed on top of a lamp. The light illuminates the models so the camera captures the difference in transmittance of model and support material. The model is kept in the chosen position by laboratory stands.

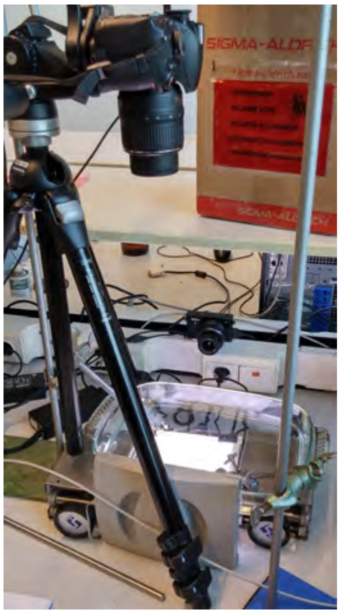

FIGURE 6.2: Measurementsetup for measuring mass change. The setup shown is used for the dissolution of the membrane containing plate.

The sizes of the models can be determined from calculating the amount of pixels which a certain path contains. The Nikon 1 J4 camera has a resolution of 5232 $\times$ 3488 pixels, the Nikon D3100 camera a resolution of 4608 $\times$ 3072. Corresponding to a resolution of 1.45 μm per pixel and 4.62 μm per pixel respectively at the distances used during the experiment. The pictures are analyzed using Matlab Image Processing.

6.2.2 Solubility

The measurements to determine the solubility of different materials, methods, solvents and geometries are discussed in this section. For the model material Fullcure 720 is used and for the support material Fullcure 705.

Ultrasonic excitation

Water jetting is the standardized method to remove the support material from the model. The solubility of the materials in water is measured in two cases. In the first case the material is soaked in water-filled regular glassware, in the second case the material is soaked in a ultrasonically excited water bath. The weight and size of the structure are measured. In this way the amount of dissolved material can be measured.

To determine the dissolving rate of Fullcure 705 boxes are used. These boxes have the size of 2.6 $\times$ 1.3 $\times$ 1.3 cm ($l \times w \times h$). The dissolving rate of Fullcure 720 is measured by dissolving cylinders with a height of 4 cm and a radius of 2 mm. The structures are measured once per twenty minutes during the dissolving process.

The measured dissolving process is fitted with equation 5.10. The measurement and fitted line can be seen in figure 6.3. Fullcure 720 did not dissolve in water, therefore the dissolution values could not be determined by fitting in a sensible way. The values found for Fullcure 705 are given in table 6.2. The boxes with Fullcure 705 dissolved layer-wise.

	$C_s(\mathrm{mg\,cm^{-3}})$ 705	$k(\mathrm{cm\,s^{-1}})$ 705
Non-Ultrasonic	27.6	424.4×10^{-3}
Ultrasonic	15.5	243.6×10^{-3}

TABLE 6.2: Dissolution values for Fullcure 705 in Ultrasonic and Non-Ultrasonic water.

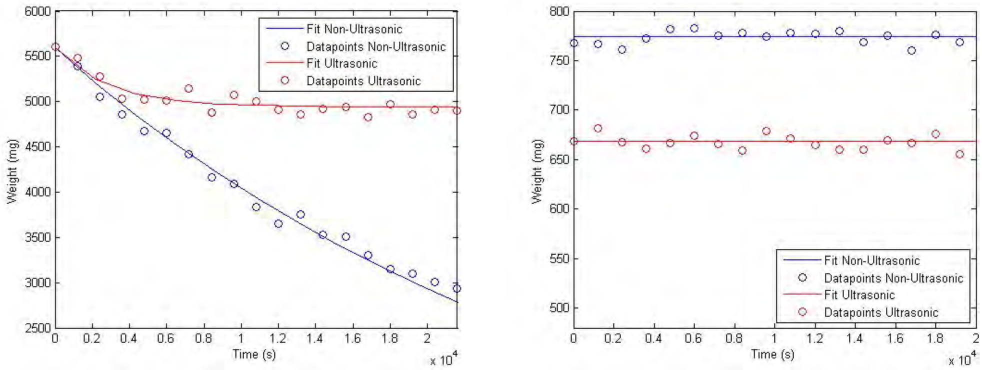

FIGURE 6.3: Dissolution of Fullcure 705 (left) and 720 (right) over time.

It can be concluded that the treatment with ultrasonic waves does not contribute to faster dissolvement of the material. Considering the approach taken with equation 5.1, we can conclude that the dissolving rate is driven by the diffusion speed of the material instead of mechanical impact on the material on this scale.

It is counter-intuitive that the measurements show a lower dissolving rate for the ultrasonic cleaning method compared to the non-ultrasonic method. Temperature differences were not monitored during the measurements. The temperature has influence on the dissolution since the diffusion coefficient is dependent on temperature according to Arrhenius equation (eq. 6.1) [28]. The measurements were done simultaneously and at the same location therefore significant differences are not expected. Identical glassware of 500 ml filled with 300 ml demineralized water were used.

$$D = D_0 e^{\frac{-E_A}{kT}} \tag{6.1}$$

Solvents

Measurements on the different solvents are done by dissolving the same boxes and cylinders as used for the ultrasonic experiment. The different solvents are; Acetone, Ethanol, Water and Potassium Hydroxide. The mass of the objects is depicted in figure 6.4, the C_s and k values of the fitted lines are given in table 6.3. Fullcure 720 absorbs acetone, therefore the weight of the object rises. It can be concluded that Fullcure 720 is resistant against many solvents. It slightly

FIGURE 6.5: Printed result of plate membranes.

dissolves in Potassium Hydroxide. Ethanol and Potassium Hydroxide are good solvents for the support material. The specificity for solving support material is best for ethanol, which will be used to dissolve the geometries.

	$C_s(\mathrm{mg\,cm^{-3}})$ 705	$k(\mathrm{cm\,s^{-1}})$ 705	$C_s(\mathrm{mg\,cm^{-3}})$ 720	$k(\mathrm{cm\,s^{-1}})$ 720
Water	27.6	424.4×10^{-6}	0.02	0.0×10^{-6}
Acetone	181.1	8.696×10^{-6}	0.04	0.0×10^{-6}
Ethanol	37.61	1789×10^{-6}	0.29	0.0×10^{-6}
Potassium Hydroxide	640.9	4.134×10^{-6}	0.01	30.5×10^{-6}

TABLE 6.3: Dissolution values for Fullcure 705 and 720 for different solvents.

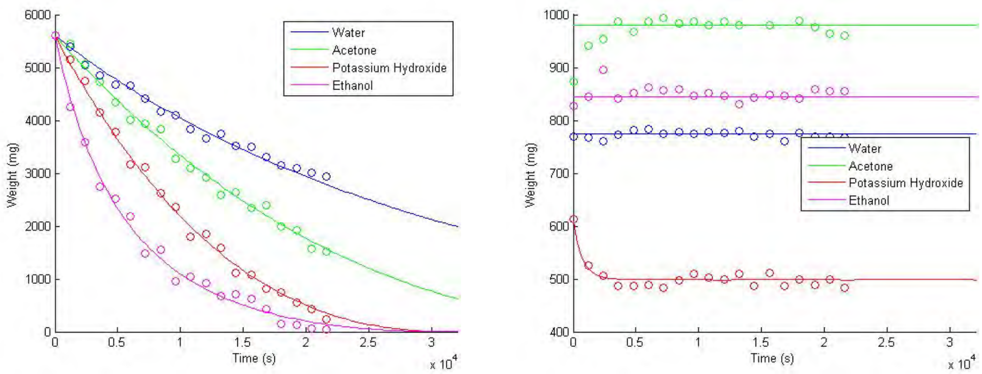

FIGURE 6.4: Dissolution of Fullcure 705 (left) and 720 (right) over time in several solvents.

6.2.2.1 Plate Membranes

The plate with membranes, as shown in figure 5.5, is printed on the Objet Eden 250. The heights of the membrane, compared to the sizes as originally designed are shown in table 6.4. The membrane as printed is shown in figure 6.5.

The printed model shows deviations with the designed computer model. The fact that the printed model is bigger then the intended model is interesting. According to the suppliers (Production Department of Materialise), no additional enlargement is done by the software. Meaning that the enlarged deviation occurs due to inaccuracy of the printer, adsorption of solvent or expanding during the fabrication process.

Membrane column	Computer model height (μm)	Printed height (μm)	Deviation (%)
1	4000	4080	2.0
2	7000	7070	1.0
3	9000	9050	0.6
4	10000	10070	0.7
5	10000	10070	0.7
6	10000	10080	0.8
7	10000	10090	0.9
8	9000	9040	0.4
9	7000	7080	1.0
10	4000	4060	1.5

TABLE 6.4: Deviations in height of the structure between the printed and computer model.

The plate dissolves according to the model, there is no layer-wise dissolving observed. The change in height of the structure is shown in figure 6.6, corresponding to the fitted model with parameters as given in 6.5 based on equation 5.5.

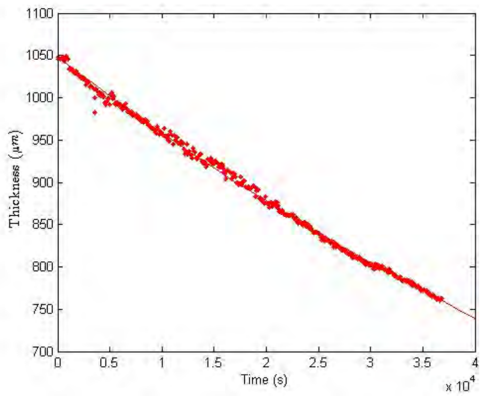

FIGURE 6.6: Thickness of model and support during dissolving in ethanol.

C_s(mg cm^{-3}) 705	k(cm s^{-1}) 705
45.80	1147×10^{-6}

TABLE 6.5: Dissolution values C_s and k for Fullcure 705 as used for the fit of the plate dissolving.

The support material in the cylindrical cavity dissolves layer-wise. The layers lie in the same plane as the membranes, which only gives a split between the rim of the cavity and the membrane. Meaning that it is more difficult for solvent to enter the underlying layers. The dissolvement in separate layers is shown in figure 6.7. In figure c differences between the flakes from the cavity above and below the membrane can be seen. The flakes above the membrane has small holes in the middle.

The cavities above and below the membrane are differently filled with support material. This difference is shown in figure 6.8. In this figure the support material is depicted in yellow and the model material in red. In the upper cavity the support material has a larger area available for dissolution than in the bottom cavity. This increases the rate of dissolution. Besides the molecular-wise dissolving, the solvent can reach all separate layers so the layers release faster. Therefore support material dissolves with a higher rate. This difference can be used as design advantage when creating such a membrane by placing the membrane non-symmetrically in the support to equal the times needed for dissolution.

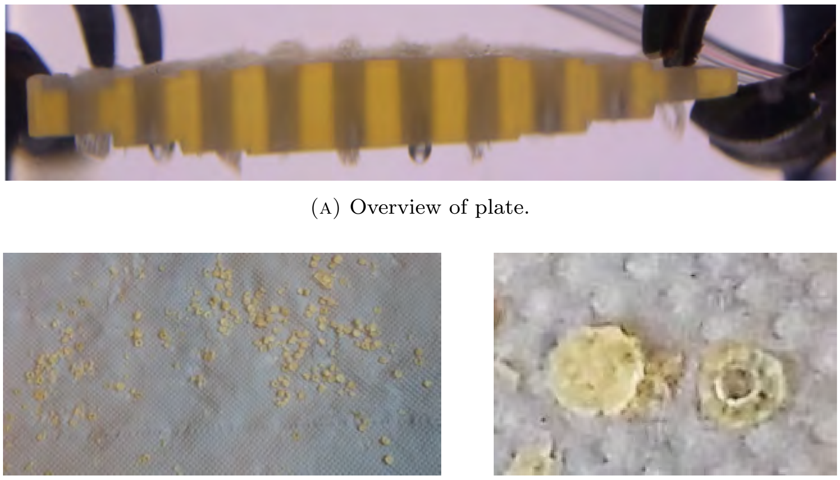

(A) Overview of plate.

(B) Cylindrical flakes from membrane cavity.

(C) Difference between flake from upper(left) and bottom(right) cavity.

FIGURE 6.7

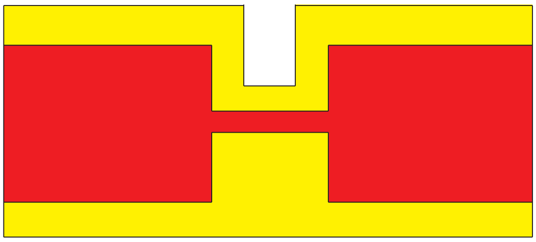

FIGURE 6.8: Difference between deposition of support material on the structure. In red the structure is depicted with the membrane in the cavity. In yellow the support material is depicted.

After 48 hours the model is totally released from its support material. Some of the membranes ruptured during the process. In figure 6.9 this process is shown for three moments in time. The plate dissolved in 10 hours, the additional 38 were needed for dissolving the support material flakes in the cavities. In this time, no decrease in thickness of the plate was observed.

The rupture of different membranes has multiple causes. Due to the flake-wise dissolving of the membrane some membranes are earlier exposed to the solvent. The membranes have various thicknesses and therefore differ in time needed to rupture. The flake-wise dissolving is hard to simulate due to the randomness in which layer has the highest chance to dissolve. The membranes released in the process will be used to determine the characteristics of the membranes.

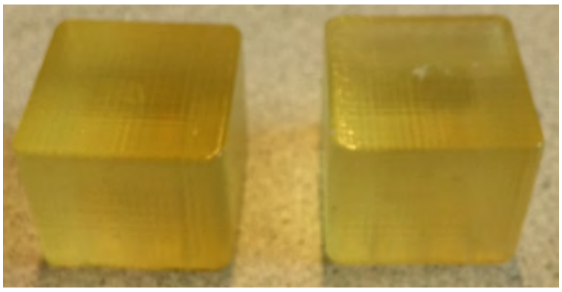

FIGURE 6.10: Cubes as printed, including support material.

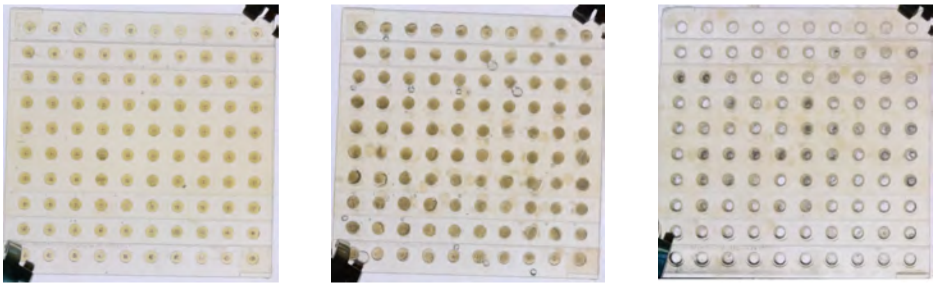

FIGURE 6.9: Process of dissolving, at time = 0, 24 and 48 hours.

During the experiment the ethanol was free to evaporate. This caused deviations in bulk volume during the first hours of the experiment. This can possibly result in a lower dissolving rate constant, due to the increase of bulk-concentration during the time of lower bulk volume. This deviation can be up to 10%.

Cubes

The printed cubes have a size of $1.02 \times 1.01 \times 1.02\,\mathrm{cm}$ $(l \times w \times h)$. A layer of $3.7\,\mathrm{mm}$ surrounding the cubes was added with support material. Notify that the deviation in size for both cubes is the same. The cubes as printed surrounded with support material are shown in figure 6.10.

The dissolving of the cubes can be seen in figure 6.11. The dissolution values are given in table 6.6. At time = $40\,000\,\mathrm{s}$ a large piece of support material was released from the structure causing the step in dissolution.

$C_\mathrm{s}(\mathrm{mg\,cm^{-3}})$ 705	$k(\mathrm{cm\,s^{-1}})$ 705
35.18	130×10^{-6}

TABLE 6.6: Dissolution values C_s and k for Fullcure 705 as used for the fit of the cube dissolving.

Cylinder

The cylinders were printed with their $z-$axis in the $x-$direction of the printer. The printed lanes lie in the y-direction as designed and the layers lay in the cylinder's $x - z$ plane. Disadvantage

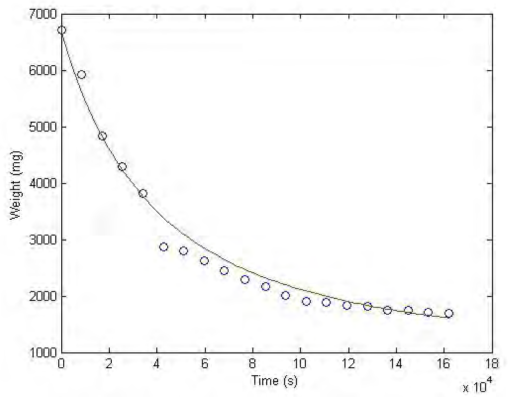

FIGURE 6.11: Dissolving of cubes surrounded with Fullcure 705.

FIGURE 6.12: Printed cylinder. The printed lanes lie in the height of the cylinder.

of this orientation is that the support material is not printed cylindrical around the cylinder. Advantage is that from earlier dissolved structures can be seen that support material dissolves in layers. In this orientation the layers have a larger volume per layer compared to the z direction design and therefore less layers. This can mean that the dissolving of the support is easier. The orientation and printed result are shown in figure 6.12.

The dissolution of the support material surrounding the model cylinder is shown in figure 6.13. The dissolution values are given in table 6.7.

$C_\mathrm{s}(\mathrm{mg\,cm^{-3}})$ 705	$k(\mathrm{cm\,s^{-1}})$ 705
31.12	24×10^{-6}

TABLE 6.7: Dissolution values C_s and k for Fullcure 705 as used for the fit of the cylindrical dissolving.

Canals

The canals printed are shown in figure 6.14. The canals were to long to dissolve uniformly. Therefore material at the edges of the canals was totally dissolved, but material in the center

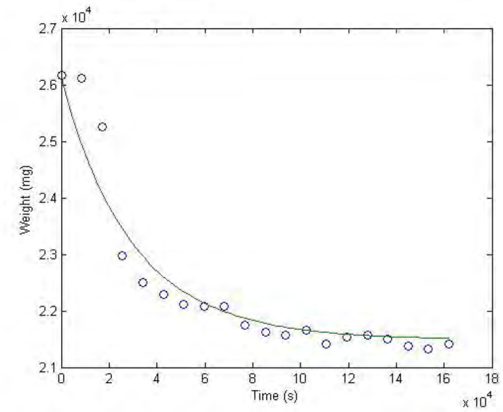

Figure 6.13: Dissolution of layer of Fullcure 705 around the cylinder.

Figure 6.14: Printed canals.

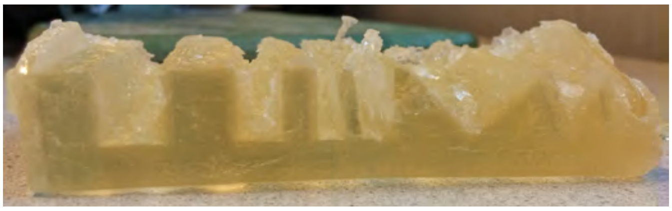

Figure 6.15: Dissolved plate with canals, in the background left over material can be seen in between the canals. In front the solvent is already dissolving the Fullcure 720.

only dissolved for 10%. Giving mountain like shapes in the canals. This process can be seen in figure 6.15. The layers of support material end at the sides of the canals. Therefore the solvent gets between the layers from the sides and solves the material at these locations. It can be seen that the solvent etches the thin parts of the model, this indicates that building thin membranes in the other planes than the $x - y$ will be difficult.

6.2.3 Conclusion

In table 6.8 the different dissolution values are compared. It can be seen that the values for k depend largely on the geometry of the model. This is due to the different path lengths of the different geometries. The experiments were done at the same location, but temperature differences can cause deviations in the measurements.

	$C_s(\mathrm{mg\,cm^{-3}})$ 705	$k(\mathrm{cm\,s^{-1}})$ 705
Plate	45.80	1147×10^{-6}
Cube	35.18	130×10^{-6}
Cylinder	31.12	24×10^{-6}

TABLE 6.8: Dissolution values C_s and k for the different geometries for dissolving Fullcure 705.

The dissolving technique can be used to release support material from the model material. When this is done it is important to avoid evaporation of the solvent. Different solvents can be used for different situations. Ethanol is a fast solvent with a high dissolution value. Potassium Hydroxide has the highest saturation concentration, which is useful in case of a larger structure, but slightly dissolves the model material. Acetone can be used as a solvent for larger structures and is less harmful to the model material. Dependent on the size of the model and the dissolution speed needed, a solvent can be chosen.

Removing support material in cavities and canals is difficult. This has to do with flakes of support material which do not leave the cavities of the material when released from the model. Here an ultrasonic bath could have an advantage. When solvent can access the edges of the support material layers, the layers can be released easier. Therefore when the support material has layers in the perpendicular plane to the solvent/material interface, support material is released faster. This can be used during the design of a model.

6.3 Membrane Characteristics

By using the described dissolution technique support material can be removed without harming the model material. The 10th of micrometer printing resolution can therefore by used to create membranes. In this section the membranes produced will be characterized and the influences of the production process will be investigated.

6.3.1 Surface of membrane

The curvature of the membrane without loading is measured with the White Light Interference Microscope (WLIM). In the case the membrane already has a curvature, non-uniform stresses exist in the membrane that cause the bending. These can come form non-uniformity of the membrane, production errors or intrinsic stresses. For the experiment the 112 μm membrane is used.

The reflection of the measurement beam on the membrane is not strong enough to detect with the WLIM. Therefore a layer of gold is added to increase the reflection. With the WLIM the deflection of the membrane is measured. First without pressure, followed by pressures of 100, 200 and 300 mbar. The profile of the membrane without pressure is given in figures 6.16 and 6.17. The support hangs over the membrane and has the shape of a cone. This cone has a

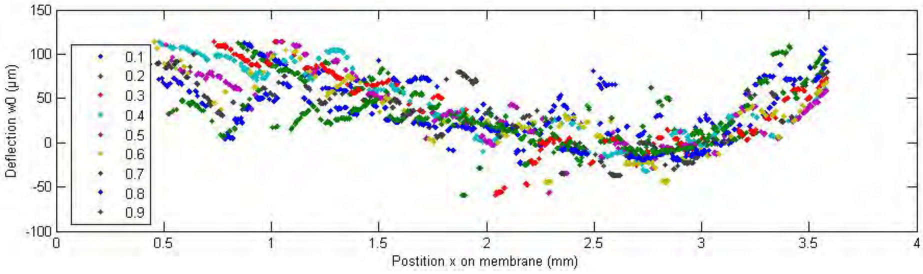

FIGURE 6.16: Height profile of membrane under WLIM. The membrane lies with an angle under the WLIM, causing height difference between the sides of the membrane. The different location points correspond with the y-lines on the membrane.

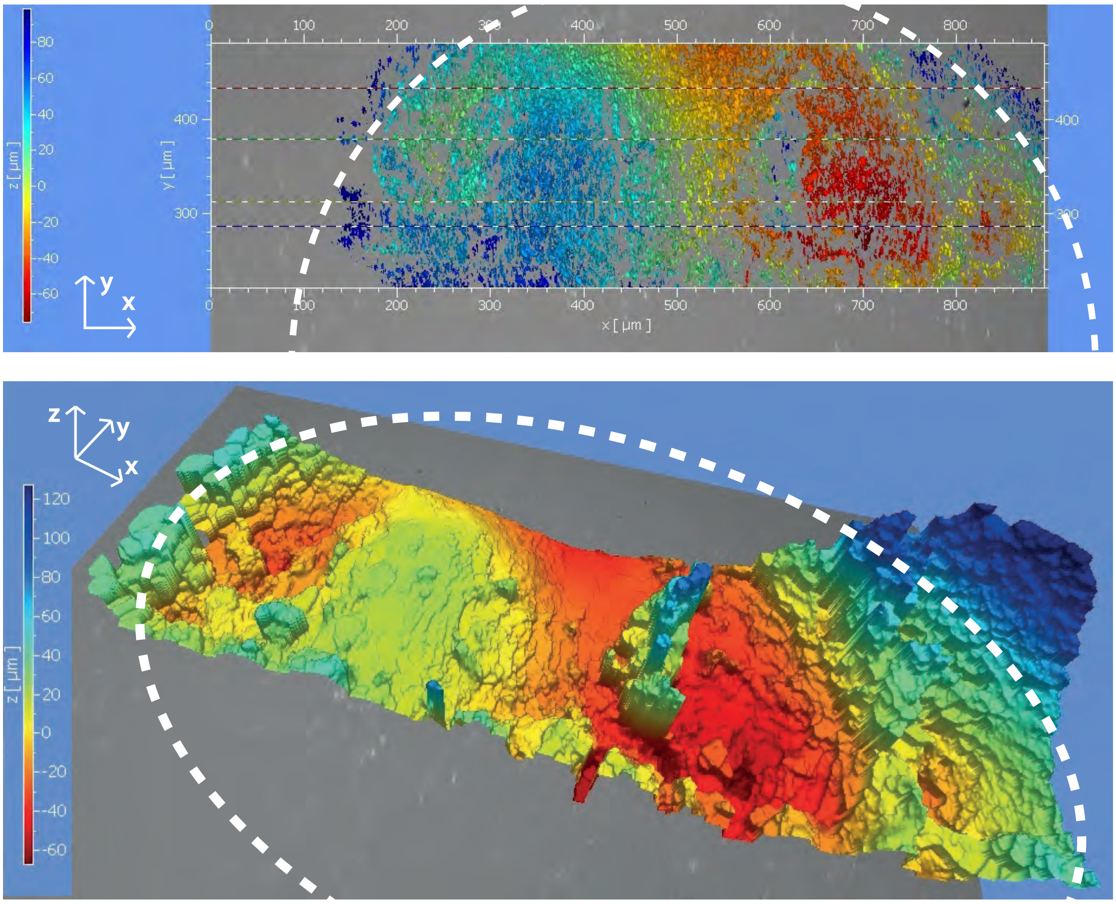

FIGURE 6.17: Membrane without pressure under WLIM. The profile of the membrane is given by the white dashed line.

smaller radius on top and a larger radius at the height of the membrane. Therefore it is not possible to focus on the full width of the membrane. From x-position 3.1 mm the membrane is shaded by the structure. The membrane is tilted to be able to focus on the membrane. This angle also causes the average difference in z between point 0 and 3.6. Traces of support material are found, giving little mountains on the membrane.

With the Scanning Electron Microscope (SEM) the cut membrane is investigated. The membrane is cut with a lancet. The pictures are shown in figure 6.18. The separate print layers are not visible in the cut. Merging of the layers can come from the cutting, heating of the membrane during sputtering of gold and merging during production. The membrane has a thickness of 112.2 μm, corresponding to the design criteria. Some left over support material can be seen, but the membrane looks homogeneous and without major errors.

Remarkable are the different canals in the wall of the model. In figure 6.18 C, small canals in the wall can be seen. These canals have the same height as the layer thickness. This means that or the solvent etched in between the layers or that the layers did not merge properly during fabrication. In figure 6.18 A larger canals are shown in the walls of the structure. These lanes are investigated with the optical microscope.

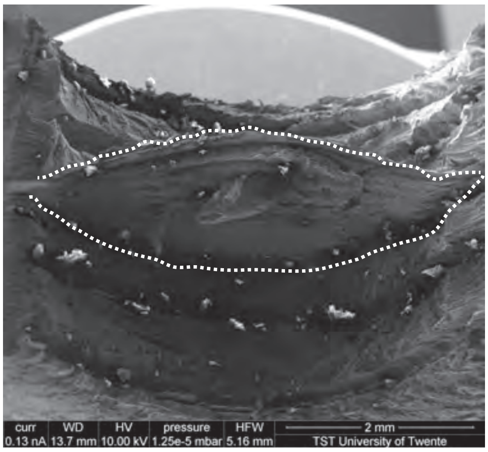

(A) Membrane non-golden side

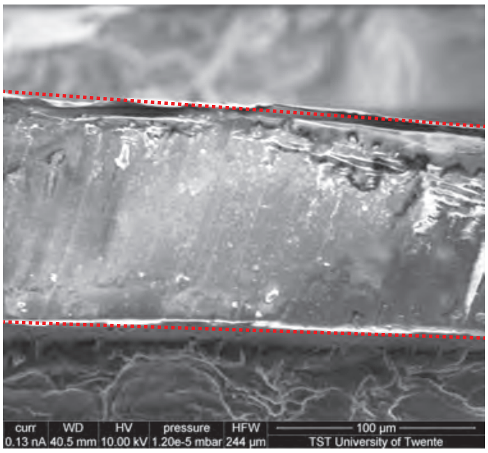

(B) Membrane cut

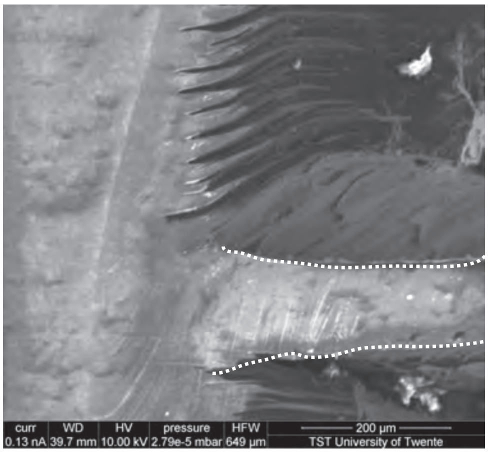

(C) Membrane support connection

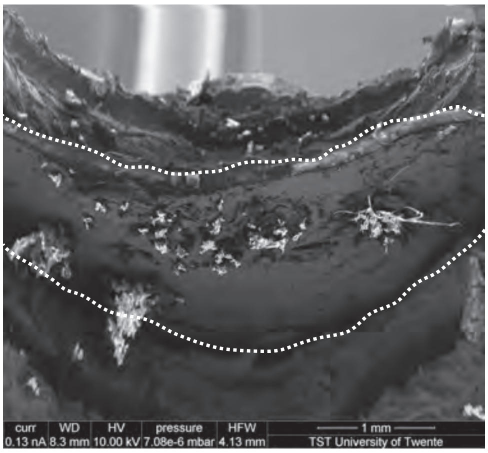

(D) Membrane golden side

FIGURE 6.18: Membrane under Scanning Electron Microscope. The membrane is shown by the dashed line.

Under the optical microscope the model is investigated on its deficiencies. In 6.19 the membrane and the support structure are shown. The layer deficiencies in the wall can not be seen due to the lower resolution of the optical microscope. In figure C and D the canals are shown. Their shape is a bit triangular and they are spread evenly over the height of the wall. There could be multiple causes for this deviation.

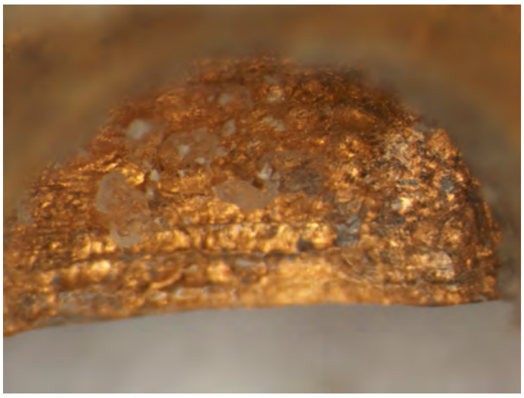

(A) Overview of golden side of the membrane

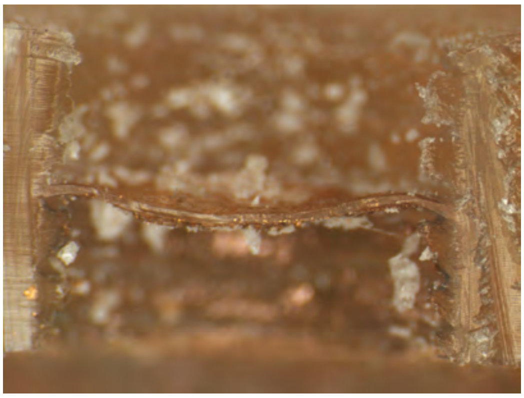

(B) Cut edge of the membrane

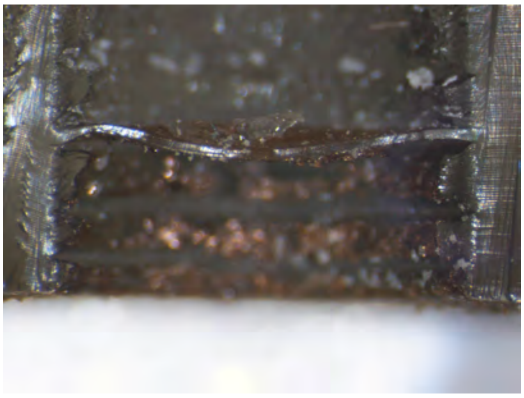

(C) Cut edge of the membrane. On the background the horizontal lines are printing deficiencies.

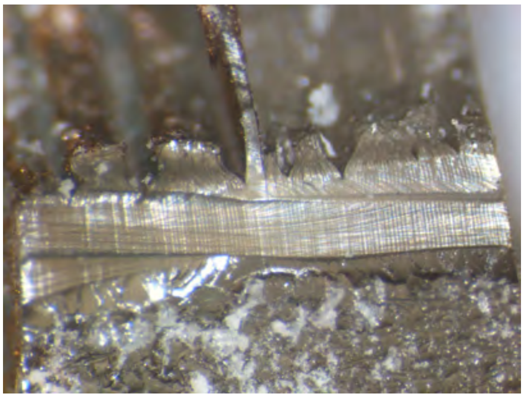

(D) The printing deficiencies in the support of the material.

Figure 6.19: Membrane under the optical microscope.

The triangulation during STL rendering could be in such a way that not a perfect cylinder is created. Computer simulations of the contour generation from the STL file does not show any deficiencies compared to the CAD model. But since the exact tolerances used by the printer are unknown, errors in this process can not be eliminated.

During the dissolution different pieces of support material were obtained. The height of these flakes of support material is $300\,\mu$m, equal to the height of the canals. These flakes consist of several layers of support material. According to Stratasys, the layer thickness is equal for support and model material. It can happen that during the printing process environmental differences cause these deviations giving less cohesion between the layers. Which can cause deviations in the printing process.

Under 300 mbar pressure the deflection is measured. The deflection is shown in figure 6.20. In figure A the measurement results are given, and the maximum deflection is found at $x = 2.59$ mm, around the center of the membrane. The membrane could not be measured totally due to shading by the rim of the support. In figure C the deflection of the membrane is compared to the to be expected curvatures for membrane and plate behavior plate. It can be seen that the membrane excites membrane behavior and thus is dominated by the stressed applied to the membrane from the support.

The maximum deflection of the membrane at 100 mbar equals 238 μm and at 300 mbar 742.20 μm. Resulting in a Youngs modulus of 1380 MPa and an intrinsic stress of 21 MPa from equations 2.39. The Poisson Ratio could not be determined, due to the lack of dynamic measurements. A Poisson ratio of 0.33 is used during the calculations.

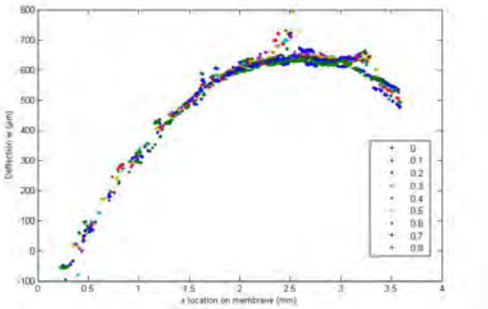

(A) Deflection versus x location

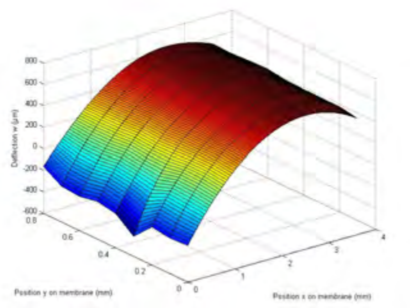

(B) 3D representation of membrane deflection

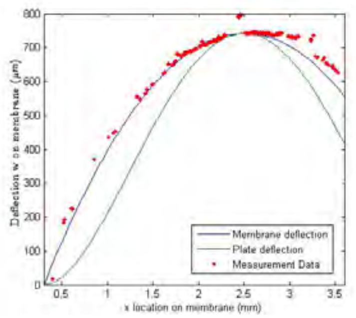

(C) Membrane versus Plate behavior

FIGURE 6.20: Membrane under 300 mbar pressure.

6.3.2 Membrane deflection

The deflection of the membrane under constant point loading is measured. For this membranes with a diameter of 5 mm and thicknesses of 112 μm, 320 μm, 352 μm, 752 μm and 768 μm. Respectively membranes 7-10, 10-2, 2-8, 7-6 and 8-5 corresponding to the membrane plate where the first index denotes the column and the second index the row.

The measurement setup is given in figure 6.21. The force is applied by a pin with a diameter of 0.6 mm, the load was centered, making use of the micro meter screw. Both sides were measured and the pin was placed in the middle. The accuracy of the location of the pin is within 10th of micrometers. Due to the displacement x applied to the membrane the scale measures a force. This force must equal force P applied at the center of the membrane. Due to the reaction force at the scale, the spring in the scale is compressed giving a displacement e of the scale.

By applying force P directly to the scale without the membrane the springs characteristics can be determined by Hooke's Law, equation 6.2. In figure 6.22 the compression of the spring of the

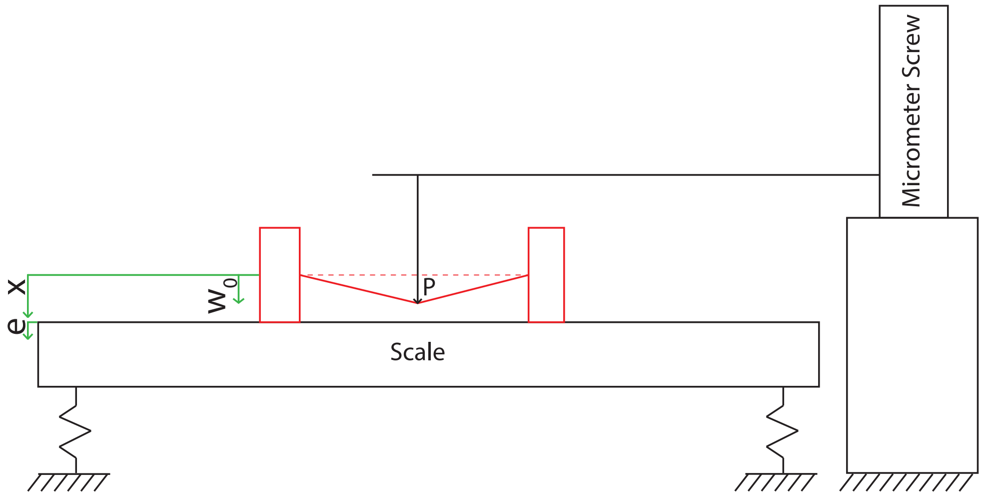

FIGURE 6.21: Measurement setup for static deviation

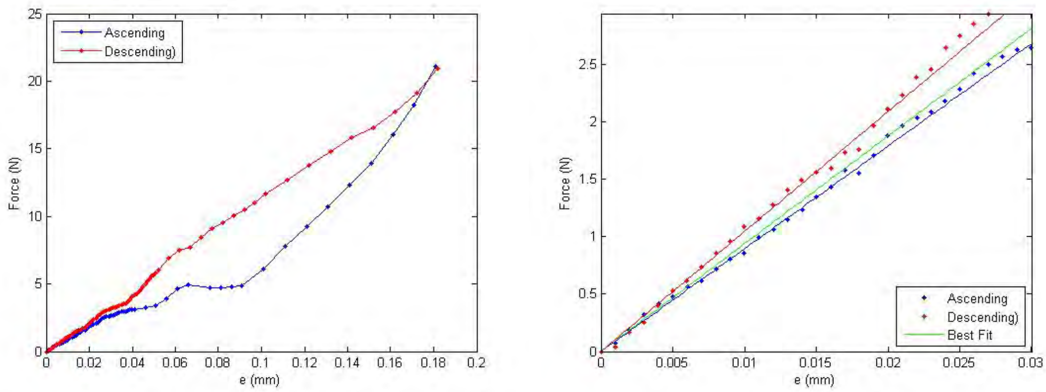

FIGURE 6.22: Left the force is plotted against e. Right a close up is given with the fitted curves for the scale.

scale is shown. For higher loads on the scale hysteresis is found, when the scale is used at forces smaller than 1.76 N, no hysteresis is found. This can be due to two different spring mechanisms in the scale used for to increase accuracy of the scale when smaller loads are applied.

$$F = ke = P \tag{6.2}$$

The deflection of the membrane is given by 6.23. From the deflection the Youngs Modulus and intrinsic stress can be calculated. This is done by fitting expression 6.3 and calculating the material properties with 6.4 and 6.5.

$$P = C_1 w + C_2 w^3 \tag{6.3}$$

$$E = \frac{3C_2 r^2 (1-\nu)}{8\pi d} \tag{6.4}$$

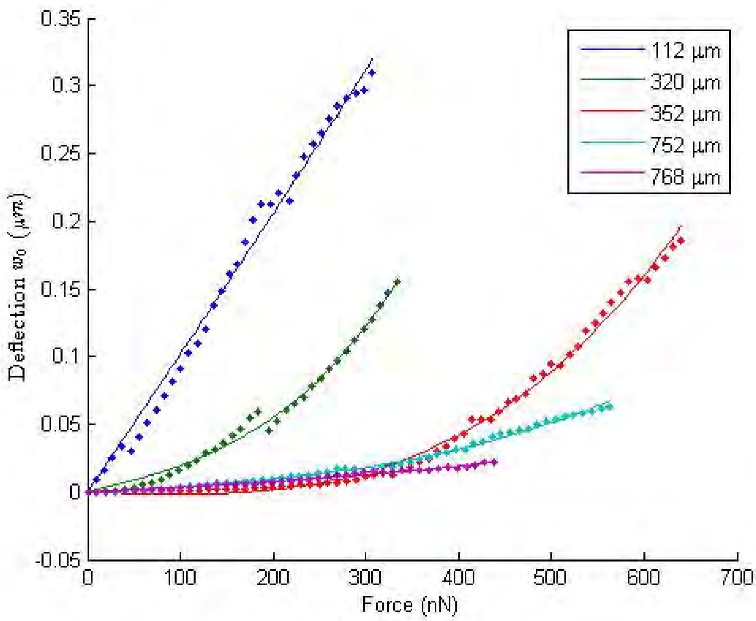

FIGURE 6.23: Deflection of membranes under constant load.

$$\sigma_T = \frac{C_1}{4\pi d} \tag{6.5}$$

The material properties of the different membranes are given in table 6.9. One of the membranes was ruptured after examination under the optical microscope. The thicker ones have a lower Youngs modulus than the thinner ones, this is due to the fact that these membranes excite plate behavior.

Membrane (μm)	E (MPa)	σ_T (MPa)	Remark
112	1360	10	Membrane behavior
320	1739	16	Membrane behavior
352	48	-2	Ruptured membrane
752	660	43	Plate behavior
768	690	16	Plate behavior

TABLE 6.9: Membrane properties.

6.3.3 Conclusion

Membranes can be created by 3D print technology. The membrane possesses a uniform thickness and bends according to a uniform membrane. The printing technology still lacks the accuracy needed to create more complex models on the micrometer scale according to their design parameters. When the walls are investigated these inaccuracies can be seen. Creating membranes is therefore not possible in other planes than the $x - y$ plane.

The rinsing of the membranes is difficult, leaving dirt on the membranes which influence the characteristics. The Youngs modulus found for the membranes are smaller than the value given in literature (2495 MPa). Its remarkable that for thicker membranes a smaller Youngs Modulus is found than for the thinner ones. The layer of gold added to the membrane 1could influence the material properties of the membrane.

Chapter 7

Conclusion and Discussion

In this report a new method for cleaning 3D printed models is explained. Solvents like acetone, ethanol and water can be used to rinse small models without harming the model material. Membranes of a few hundreds micrometers are produced to give a prove of concept and material properties of this membrane are determined.

Ethanol is the most suitable solvent for dissolving the support material. Ethanol has a dissolution rate k of $1.789 \times 10^{-3}\,\mathrm{cm\,s^{-1}}$ and a saturation concentration $C_s = 37.61\,\mathrm{mg\,cm^{-3}}$. This corresponds to 18.81 gram per 500 ml. When larger models need to be dissolved other solvents can give better results. One of these solvents is acetone, with a much lower dissolution rate but a higher saturation concentration of $181.1\,\mathrm{mg\,cm^{-3}}$. In this research all support material was dissolved using a single solvent. Two different dissolution steps could be beneficial, by for example first removing the larger pieces of support material. The model for dissolving does not account for layer-wise dissolution. Therefore saturation concentrations and dissolution rate constants can deviate from their true value.

The printing technique evolves and over time gives possibilities to print even smaller structures. When printers without the use of support material can print the same resolutions as the Polyjet technology, better membranes could be made. When creating membranes smaller than $800\,\mu\mathrm{m}$ it is important to place them asymmetrical in the cavity to increase dissolving efficiency. They must be placed lower than the middle of the cavity to equalize the dissolution times in the upper and bottom cavity.

The membrane can be created according to the design criteria. The thinnest membrane released is $112\,\mu\mathrm{m}$ thick. This membrane has a uniform thickness, but it is difficult to remove the last traces of support material without rupture of the membrane. The Youngs modulus of the material measured by static deflection with a point load is 1360 MPa, with a uniform pressure 1380 MPa. In the latter case a layer of gold of 100 nm is added, which can influence the material properties. The intrinsic stress is measured to be 16 MPa and 21 MPa by the point and uniform loading measurement methods respectively.

The stage of STL conversion adds uncertainty in the model. Current design tools make use of fully defined CAD models. It would be an improvement if printers would directly read-out these CAD files. It is strange that STL-file is the industry standard, when the engineering field switches to fully defined models.

3D printing has promising possibilities to create complex membranes and other small scale models. The current effect of small scale printing is still ill defined and precision needs to be increased to create well-designed membranes. Thin layers can be produced and released with the method described in this report. Simple membranes can be created on this scale with 3D print technology. When more complex membranes are produced, the many inaccuracies of the technology will make the design less predictable. The various unknown parameters and problems revealed in this report indicate that still a lot of research needs to be done on creating structures on this scale. The membranes as intended in this report can be fabricated by making use of 3D print technology.

Appendix A

Contacts

The following persons did a remarkable job on helping printing the structures and I would like to thank them for their support:

Dennie Rijk
Layertec B.V.
+31 (0) 418 644 696
drijk@layertec.nl
www.layertec.nl

Olga Yatsenko
Materialise Belgium
+32 16 39 66 11
contact@i.materialise.com
www.materialise.com

Han Wopereis
Chair Robotics and Mechatronics
3dprinter-ram@utwente.nl

Bibliography

[1] J.F.C Windmill, S Bockenhauer, and D Robert. Time-resolved tympanal mechanics of the locust. *Journal of The Royal Society Interface*, 5(29):1435–1443, 2008. ISSN 1742-5689. doi: 10.1098/rsif.2008.0131.

[2] P.J. Westerik. Mems acoustic sensors inspired by the locus ear, 2014.

[3] Axel Michelsen. The physiology of the locust ear. *Zeitschrift für vergleichende Physiologie*, 71(1):102–128, 1971. ISSN 0044-362x. doi: 10.1007/BF01245156. URL `http://dx.doi.org/10.1007/BF01245156`.

[4] Robert Malkin, Thomas R. McDonagh, Natasha Mhatre, Thomas S. Scott, and Daniel Robert. Energy localization and frequency analysis in the locust ear. *Journal of The Royal Society Interface*, 11(90), 2013. ISSN 1742-5689. doi: 10.1098/rsif.2013.0857.

[5] Wikipedia. Fused deposition modeling: 1 – opbrengen (injectie) van gesmolten materiaal, 2 – vorm in opbouw. 3 – beweegbaar platform, March 2015. URL `http://nl.wikipedia.org/wiki/Fused_deposition_modeling#/media/File:FDM_by_Zureks.png`.

[6] 3D printing industry. The free beginners's guide to 3d printing. URL `3dprintingindustry.com`.

[7] Werner Soedel. *Vibrations of Shells and Plates*. MARCEL DEKKER, INC., 1981. ISBN 0-8247-1193-9.

[8] Steven Lehar. The world in your head, figure 8.6, May 2015. URL `http://cns-alumni.bu.edu/~slehar/webstuff/book/fig8.6.html`.

[9] Tom Irvine. Natural frequencies of circular plate bending modes, February 2012.

[10] W.K. Schomburg. *Introduction to Microsystem Design*. Springer-Verlag Berlin Heidelberg, 2011. doi: 10.1007/978-3-642-19489-4.

[11] Dassault Systèmes SolidWorks Corp. Solidworks, version 2014a, 2014. URL `http://www.solidworks.com/`.

[12] I. Stroud and P.C. Xirouchakis. {STL} and extensions. *Advances in Engineering Software*, 31(2):83 – 95, 2000. ISSN 0965-9978. doi: http://dx.doi.org/10.1016/S0965-9978(99)00046-0. URL `http://www.sciencedirect.com/science/article/pii/S0965997899000460`.

[13] 3D Print Company. Pa2200 datasheet, concept laser m3 datasheet, February 2015. URL http://www.3dprintcompany.nl.

[14] Leapfrob BV. High quality and affordable 3d printers, February 2015. URL http://www.lpfrg.com.

[15] Matbase. Matbase, digital material database, March 2015. URL http://www.matbase.com/material-categories/natural-and-synthetic-polymers/commodity-polymers/material-properties-of-acrylonitrile-butadiene-styrene-general-purpose-gp-abs.html#properties.

[16] Materialise. Details polyjet digital materials, Oktober 2013. URL http://manufacturing.materialise.com/sites/default/files/public/AMS/Updated%20datasheets/ams_datasheets_polyjet_0.pdf.

[17] 3Dprinter.nu. Polyjet methode, March 2015. URL http://www.3dprinter.nu/fig/polyjet_machine.jpg.

[18] J. Siepmann and F. Siepmann. Mathematical modeling of drug dissolution. *International Journal of Pharmaceutics*, 453(1):12 – 24, 2013. ISSN 0378-5173. doi: http://dx.doi.org/10.1016/j.ijpharm.2013.04.044. URL http://www.sciencedirect.com/science/article/pii/S0378517313003451. Poorly Soluble Drugs.

[19] A.A. Noyes and W.R. Whitney. The rate of solution of solid substances in their own solutions. *J. Am. Chem. Soc*, 19:930-934, 1897.

[20] H. Mehrer. *Diffusion in Solids: Fundamentals, Methods, Materials, Diffusion-Controlled Processes*. Springer Series in Solid-State Sciences. Springer, 2007. ISBN 9783540714880. URL https://books.google.nl/books?id=IUZVffQLFKQC.

[21] M.W. Zemansky and R. Dittman. *Heat and Thermodynamics: An Intermediate Textbook*. International Series in Pure and Applied Physics. McGraw-Hill, 1997. ISBN 9780070170599.

[22] Jordi Labs. Polymer solubility index, March 2015. URL http://www.lifescience.ca/DATA/CATALOGUE/211~v~Polymer_Solubility_Index.pdf.

[23] Wikipedia. Propylene glycol, March 2015. URL http://en.wikipedia.org/wiki/Propylene_glycol.

[24] C. Zelig A. Mishek F. Larsen, N. Henke et al. Linked-in discussion on removing support material, March 2015. URL https://www.linkedin.com/groups/Objet-support-solvent-Can-you-123610.S.82031711.

[25] Objet Geometries Ltd. Models cleaning procedure usign naoh (sodium hydroxide), March 2015. URL http://www.tritech3d.co.uk/images/contentitems/67_1_1.pdf.

[26] Wikipedia. White light interferometry, March 2015. URL http://en.wikipedia.org/wiki/White_light_interferometry.

[27] Anindya Chatterjee. An introduction to the proper orthogonal decomposition. *Current science*, 78(7):808–817, 2000.

[28] E.L. Cussler. *Diffusion: Mass Transfer in Fluid Systems*. Cambridge Series in Chemical Engineering. Cambridge University Press, 2009. ISBN 9780521871211. URL `http://books.google.nl/books?id=dq6LdJyN8ScC`.